A CENSUS OF THE SUPERSOFT X-RAY SOURCES IN M31

Marina Orio[1,2], Thomas Nelson[3,4], Antonio Bianchini[5], Francesco Di Mille[5], and Daniel Harbeck[6]
[1] INAF-Osservatorio Astronomico di Padova, vicolo Osservatorio, 5 I-35122 Padova, Italy
[2] Department of Astronomy, University of Wisconsin-Madison, 475 N. Charter St., Madison, WI 53706, USA; orio@astro.wisc.edu
[3] Department of Physics, University of Maryland, Baltimore County, 1000 Hilltop Circle, Baltimore, MD 21250, USA
[4] CRESST and X-ray Astrophysics Laboratory, NASA Goddard Space Flight Center, Greenbelt, MD 20771, USA
[5] Dipartimento di Astronomia, Università di Padova, vicolo Osservatorio, 2, I-35122 Padova, Italy
[6] National Optical Astronomy Observatory, WIYN Observatory, 950 N. Cherry Avenue, Tucson, AZ 85726, USA
Received 2009 September 3; accepted 2010 May 12; published 2010 June 17

ABSTRACT

We examined X-ray, ultraviolet, and optical archival data of 89 supersoft X-ray sources (SSS) in M31. We studied the timescales of X-ray variability and searched UV and optical counterparts. Almost a third of the SSS are known classical or recurrent novae, and at least half of the others exhibit the same temporal behavior as post-outburst novae. Non-stellar objects among SSS seem to be rare: less than 10% of the classified SSS turned out to be supernova remnants, and only one source has been identified with an active galactic nucleus in the background. Not more than 20% of the SSS that are not coincident with observed novae are persistent or recurrent X-ray sources. A few of these long-lasting sources show characteristics in common with other SSS identified as white dwarf (WD) close binaries in the Magellanic Clouds and in the Galaxy, including variability on timescales of minutes, possibly indicating the spin period of a WD. Such objects are likely to be low-mass X-ray binaries with a massive WD. A third of the non-nova SSS are in regions of recent star formation, often at the position of an O or B star, and we suggest that they may be high-mass X-ray binaries. If these sources host a massive hydrogen-burning WD, as it seems likely, they may become Type Ia supernovae (SNe Ia), constituting the star formation dependent component of the SNe Ia rate.

Key words: binaries: close – galaxies: individual (M31) – galaxies: stellar content – ultraviolet: stars – white dwarfs – X-rays: stars

Online-only material: color figures

1. INTRODUCTION

Supersoft X-ray sources (SSS), first discovered with the *Einstein* satellite in the Magellanic Clouds (Long et al. 1981), are soft, luminous X-ray sources, with bolometric luminosity from 10^{36} to a few times 10^{38} erg s^{-1}. The spectrum can be fitted with a blackbody at a temperature in the range of 10^5–10^6 K. Thanks to their high absolute luminosity, most SSS are discovered in external galaxies, both in the Local Group and farther afield, that lie at high galactic latitudes and therefore have lower absorption along the line of sight (Di Stefano et al. 2003; Pietsch et al. 2004). Average measured fluxes are low and the sources are selected through X-ray hardness ratio criteria (e.g., Di Stefano & Kong 2003), so the classification is heterogeneous, and encompasses a variety of objects including a few young supernova remnants (SNRs; see Orio 2006). However, the majority of SSS identified at other wavelengths in the Galaxy and in the Magellanic Clouds are extremely hot white dwarfs (WDs). Although some of these WDs are isolated, such as the central stars of planetary nebulae or the hottest PG 1159 stars, most seem to be in binary systems, where the source of the supersoft X-rays is an accreting WD burning hydrogen in a shell on its surface. Binary SSS include post-outburst classical and recurrent novae and non-nova systems such as CAL 83 in the LMC (van den Heuvel et al. 1992). Recurrent novae, which eject little mass in an outburst and appear as SSS for few months every 10–50 years (e.g., RS Oph; Nelson et al. 2008 and references therein), and semi-permanent SSS, in which steady surface nuclear burning allows the WD to grow in mass with time (e.g., van den Heuvel et al. 1992), represent two viable single degenerate channels to Type Ia supernovae (SNe Ia). Alternatively, the end point may be a neutron star produced by an accretion-induced collapse.

The progenitors of SNe Ia have never been observed before the supernova explosion; however it has been established that SNe Ia are the thermonuclear disruptions of a carbon-oxygen (CO) WD close to or at the Chandrasekhar mass (see review by Hillebrandt & Niemeyer 2000 and references therein). The light curve is powered by the decay of ^{56}Ni in the ejecta (Arnett 1979), so the peak luminosity is remarkably homogeneous, averaging $M_B \simeq -19.4$ (Branch 1998). The evolutionary scenarios leading to SNe Ia can be broadly divided into two classes—single and double degenerate (Yungelson 2005; Parthasarathy et al. 2007). In single degenerate models, the WD accretes material from a main sequence or giant companion via Roche lobe overflow or wind accretion. The system explodes when enough mass is accreted that the WD reaches the Chandrasekhar limit. In double degenerate models, two WDs with combined mass exceeding the Chandrasekhar limit merge and explode. The single degenerate model is appealing because it is more likely to lead to the required explosion, in contrast with the double degenerate merger scenario which is more likely to end in an accretion-induced collapse producing a neutron star (e.g., Nomoto & Iben 1985; Saio & Nomoto 2004). We know a large class of accreting WD binaries—cataclysmic variables (CVs)—but the vast majority of these systems do not host sufficiently massive WDs to ever reach the Chandrasekhar limit. Instead, a large number of double degenerate systems culminate in two WDs with a total mass exceeding the limit. The double degenerate model also offers a simple explanation for the lack of hydrogen observed in SNe Ia. Unfortunately, binary WDs are difficult to observe because of their low luminosity, and therefore the predictions of the theory are difficult to test.

The SNe Ia rate appears to depend on the morphology and star formation rate (SFR) of the host galaxy. The brightest

SNe Ia seem to be only in galaxies that are still undergoing star formation (e.g., Hamuy et al. 1995; Mannucci et al. 2005). Mannucci et al. (2005) claimed that the SNe Ia rate is highest in the bluest galaxies, i.e., those with active star formation. Sullivan et al. (2006) found evidence that the SN Ia rate scales with the specific star formation rate (sSFR) of the host galaxy, and claim that a subset of SNe Ia occurs in the youngest stellar populations. These authors also suggest that the brightest supernovae occur in the galaxies with highest sSFR. The progenitor evolutionary models must account for these differences. In a recent paper, Gilfanov & Bogdan (2010) claim that the integrated supersoft X-ray flux in the unresolved core of M31 and of several elliptical galaxies does not account for more than 5% of the SNe Ia rate, assuming that SSS remain luminous X-ray sources for 10^7 years. These authors thus implicitly rule out that steady burners with a relatively massive (1–2 $M_\odot$ secondary, like CAL 83) are the main class of SNe Ia progenitors in the galaxies they examined. However, we note that the expected integrated supersoft X-ray flux would be even several orders of magnitudes lower, and thus perfectly consistent with the authors' upper limit, if single degenerate progenitors are not detectable as SSS for most of the life of the systems. This is the case of recurrent novae like RS Oph (see Nelson et al. 2008, and references therein) or U Sco (see Hachisu & Kato 2000, and references therein), which are visible as SSS for ≃two months every 10–30 years. Recurrent novae, in which the atmosphere is not transparent to supersoft X-rays until after each outburst for only a couple of months, and symbiotics, in which the SSS may be intrinsically obscured by nebular material for most of the life of the systems, are actually the favored single degenerate SNe Ia candidates (Parthasarathy et al. 2007), rather than CAL 83 type systems (as studied by van den Heuvel et al. 1992). We intend to contribute to this ongoing, lively discussion, by studying SSS in M31 as point sources and by identifying their characteristics, including their duty cycle as SSS.

Fifteen SSS have been observed and classified in the Magellanic Clouds, and several more SSS candidates were detected with very low signal-to-noise ratio (S/N; Greiner 1996, 2000; Haberl et al. 2000; Šimon 2003). There is clear-cut observational evidence that at least five of the LMC sources and three in the SMC are accreting WDs in close binaries, including Novae 1995 and 2009 in the LMC (transient SSS; Orio et al. 2003, 2009) and two SMC symbiotics (apparently permanent SSS; see Orio et al. 2007).

The largest known population of SSS has been discovered in M31, the most massive member of the local group, with *ROSAT* (Supper et al. 1997; Kahabka 1999; Greiner et al. 2004), *Chandra* (Di Stefano & Kong 2003, 2004), and *XMM-Newton* (Pietsch et al. 2005a; Orio 2006; Stiele et al. 2008). Except for a few SNRs, the SSS that have been identified are all post-outburst novae (Nedialkov et al. 2002; Pietsch et al. 2005a, 2007; Orio 2006). In this project, we have updated the X-ray database of the SSS in M31. Our final goal is to find the connection between the M31 SSS and WDs, and determine in what type of binaries the WDs are. To proceed in this direction, we examined all the available literature and also discovered a few new SSS. We studied the long-term time X-ray variability of the M31 SSS, and carried out a multi-wavelength study using all the available UV and optical archival data, and some new, deep optical images.

A fundamental criterion for identifying the WDs among the SSS is their absolute luminosity, thus we need to know the distance. A clue to identifying a WD is if we can establish that a source is located in M31 and is not an SNR, as we know

that there are no other stellar objects that become as hot and luminous as accreting and hydrogen-burning WDs. However, we need to examine three other possibilities of objects in the fore- and background. WDs in polar systems have blackbody-like emission from the polar caps, but they have a much lower L_x/L_{opt} ratio than hydrogen-burning WDs. The optical counterparts would be observable in the foreground. Cooling neutron stars are not much hotter than WDs, but they are four orders of magnitudes less luminous, therefore they would also be in the Galaxy. Finally, active galactic nuclei (AGNs) seldom appear as SSS, but they cannot be ruled out.

A secondary criterion for finding WD binaries among our SSS sample is the temporal variability. First of all, the classical or recurrent novae among them have a very characteristic X-ray and optical light curve. Often, they also exhibit variations on minute timescales, which are attributed to either the spin of the WD or to non-radial pulsations (e.g., Drake et al. 2003; Leibowitz et al. 2006; Nelson et al. 2008). The variability of other SSS WD binaries in the MC has also already been well monitored. Therefore, the temporal behavior gives excellent clues on the nature of the objects.

2. SUPERSOFT SOURCES IN M31

M31 has been monitored extensively in X-rays over the last decade, so we can now address questions concerning transient behavior, recurrence time, and duty cycle of the SSS population.

To look for new SSS, and to evaluate the long-term behavior of the previously known systems, we searched the HEASARC database for all observations of M31 carried out with *Chandra*, *XMM-Newton,* and *Swift* since the studies mentioned above. Not all available observations are useful for our purposes, since some monitoring exposures are too short (e.g., most of the *Swift* exposures). Moreover, many X-ray observations of M31 are done with the *Chandra* HRC-I, which has almost no spectral resolution and therefore cannot be used to discover new SSS, but only to follow up previously discovered ones. Many more observations of the core were done with ACIS-I, which is not sensitive below 0.5 keV and detects only the most luminous soft SSS. We examined the ACIS-I observations only to follow up specific, known sources. Table 1 lists the new public X-ray observations that were not included in papers written specifically on SSS. For completeness, we also re-examined a few long *ROSAT*-PSPC pointings (not part of the surveys) analyzed by Greiner et al. (2004), the *Chandra* ACIS-S observations of the peripheral SSS (observation numbers from 2048 to 2054), and the deep ACIS-S image of the center obtained by Di Stefano et al. in 2001–2002 (Di Stefano et al. 2004; Greiner et al. 2004). We included all the *Swift* observations longer than 6 ks, and also a few shorter ones carried out in the late spring or summer of 2008, in order to explore the possibility of detecting new SSS even in short exposures, although we did not find them.

In M31, SSS are usually identified using X-ray hardness ratio criteria, since the number of photons detected for each source is often too low for spectral analysis. The criterion in the literature varies with X-ray telescope, depending on the spectral response of the individual instrument, and also with author—for instance, the selection criterion used by Pietsch et al. 2005a for the *XMM-Newton* images of M31 differs from the one used by Orio (2006), developed to more closely match the *Chandra* ACIS selection procedure used by Di Stefano et al. (2003, 2004). In Table 2, we included all SSS previously classified as such, regardless of the details of the selection, in order to present a very comprehensive

Table 1
New X-ray Exposures of M31

Obs. ID	Target	R.A. (J2000.0)	Decl. (J2000.0)	Exposure Time (ks)	Date
XMM-Newton					
0112570501	Core	00 44 46.36	+41 23 14.3	MOS 5	2000 Jun 25
0112570701	Core	00 42 39.06	+41 14 55.9	4	2003 Feb 8
0109270801	North2	00 44 42.0	+42 08 47.4	60	2002 Jan 26
0202230201	RX J0042.6+4115	00 42 42.12	41 16 57.1	20	2004 Jul 16
0202230301	RX J0042.6+4115	00 42 42.08	41 16 56.9	29	2004 Jul 17
0202230401	RX J0042.6+4115	00 42 42.26	41 16 58.2	22	2004 Jul 18–19
0202230501	RX J0042.6+4115	00 42 42.23	41 16 57.6	27	2004 Jul 16
0403530201	Bo375	00 45 49.6	+41 40 29.5	MOS 13	2006 Jul 8
0403530301	Bo375	00 45 49.46	+41 40 33.3	MOS 18	2006 Jul 10
0403530401	Bo375	00 45 49.3	+41 40 35.5	MOS 16	2006 Jul 12
0403530501	Bo375	00 45 49.28	+41 40 33.7	MOS 15	2006 Jul 14
0403530601	Bo375	00 45 49.32	+41 40 33.8	MOS 18	2006 Jul 16
0402560101	S3	00 38 56.9	+40 15 47.2	61	2006 Jun 28
0402560201	M 31 SS1	00 43 32.92	+40 55 58.0	63	2006 Jun 30
0402560301	NN3	00 44 42.00	+42 08 47.4	60	2007 Jan 3
0402560401	SS2	00 42 20.63	+40 38 04.0	59	2006 Jul 8
0402560501	N2	00 38 58.20	+40 37 04.0	39	2007 Dec 31
0402560601	SS3	00 40 48.58	+40 21 57.5	59	2007 Dec 25
040256070	SN3	00 39 05.62	+40 38 43.7	66	2007 Jul 23
0402560801	S2	00 40 01.5	+40 34 40.1	66	2006 Dec 25–26
0402561001	NS1	00 44 46.36	+41 23 14.3	66	2006 Dec 30–31
0402561101	NN2	00 43 05.63	+41 54 20.5	61	2007 Jan 1
0402561201	NS2	00 45 38.99	+41 31 00.1	63	2007 Jan 2
0402451501	N1	00 46 34.32	+41 53 08.3	63	2007 Jan 1
040256140	NS3	00 46 34.43	+41 53 10.2	64	2007 Jan 4
0402561801	S2	00 40 01.52	+40 34 40.0	8	2006 Dec 26
040256190	NS2	00 45 38.92	+41 31 00.3	8	2007 Mar 1
0402562001	NS3	00 46 34.32	+41 53 08.3	8	2007 Jan 5
0405320501	M31	00 42 48.49	+41 16 57.6	22	2006 Jul 2
0405320701	M31	00 42 40.43	+41 15 19.9	16	2006 Dec 31
0405320801	M31	00 42 40.82	+41 15 14.2	14	2007 Jan 16
0405320901	M31	00 42 41.76	+41 15 08.2	17	2007 Feb 5
0505760101	S3	00 38 55.72	+40 15 57.	59	2007 Jul 24
0405320301	M31	00 42 40.81	+41 15 14.2	14	2007 Jan 16–17
0405320701	M31	00 42 40.81	+41 15 14.2	14	2007 Jan 16–17
0405320801	M31	00 42 40.81	+41 15 14.2	14	2007 Jan 16–17
0505760201	M 31 SS1	00 43 32.12	+40 56 09.3	58	2007 Jul 22
0505760301	SS2	00 42 12.46	+40 36 23.1	46	2007 Dec 28
0505760501	SN3	00 38 58.20	+40 37 00.4	39	2007 Dec 31
0511380201	M 31 SS1	00 43 25.14	+40 54 20.6	29	2008 May 5
0511380301	M31	00 39 37.12	+40 57 57.9	36	2008 Jan 1
0511380601	M 31 SS1	00 43 26.54	+40 54 09.4	30	2008 Sep 2
0505720201	M31	00 42 40.18	+41 15 20.3	27	2007 Dec 27
0505720401	M31	00 42 40.18	+41 15 20.3	27	2008 Jan 8
0505720501	M31	00 42 41.29	+41 15 11.9	22	2008 Jan 27
0505720601	M31	00 42 42.01	+41 15 06.8	22	2008 Feb 7
0560180101	N2007-12b	00 43 19.9	+41 13 46.6	22	2008 Jul 18
Chandra ACIS-S					
313	M31 trans.	00 42 40.80	+40 51 54.0	6	2000 Sep 21
314	M31 trans.	00 42 40.80	+40 51 54.0	5	2001 Oct 21
4536	RX J0041.7+4056	00 41 49.20	+40 56 43.0	55	2006 Mar 8
5690	M32	00 42 41.80	+40 51 41.8	116	2002 May 27
2494	M31	00 42 41.80	+40 51 52.0	17.9	2002 Aug 6
2017	M32	00 42 41.80	+40 51 41.8	51	2002 Aug 06
Chandra ACIS-I					
1575	M31 nucleus	00 42 42.30	+41 16 08.4	38	2002 Oct 11
1580	M31 nucleus	00 42 40.80	+40 51 54.0	5	2000 Nov 17
1584	M31 nucleus	00 42 37.50	+40 54 27.0	5	2001 Jul 3
Chandra HRC-I					
247	M31-South 2	00 40 27.00	+40 40 12.0	2	2001 May 8
259	M31-South	00 42 08.00	+40 55 17.0	2.5	2000 Mar 8
260	M31-South 1	00 42 40.80	+40 51 54.0	1.2	2000 May 26
265	M31-South 1	00 42 40.80	+40 51 54.0	1.2	2001 Feb 4

Table 1
(Continued)

Obs. ID	Target	R.A. (J2000.0)	Decl. (J2000.0)	Exposure Time (ks)	Date
1912	M31	00 42 42.30	+41 16 08.4	50	2001 Oct 31
3813	BO 375	00 45 58.58	41 39 55.7	5	2003 Oct 10
5925	M31	00 42 44.40	+41 16 08.3	47	2004 Dec 06
5926	M31	00 42 44.40	+41 16 08.3	28	2004 Dec 27
5927	M31	00 42 44.40	+41 16 08.3	27	2005 Jan 28
5928	M31	00 42 44.40	+41 16 08.3	45	2005 Feb 21
6177	M31	00 42 44.40	+41 16 08.3	20	2005 Dec 29
7283	M31	00 42 44.30	+41 16 09.4	20	2006 Jun 5
7284	M31	00 42 44.30	+41 16 09.4	20	2006 Sep 30
8526	M31	00 42 44.30	+41 16 09.42	20	2007 Nov 7
8527	M31	00 42 44.30	+41 16 09.4	20	2007 Nov 7
8528	M31	00 42 44.30	+41 16 09.4	20	2007 Nov 28
8529	M31	00 42 44.30	+41 16 09.4	19	2007 Dec 7
8530	M31	00 42 44.30	+41 16 09.4	19	2007 Dec 17
9528	M31	00 42 44.30	+41 16 09.4	20	2008 Nov 28
4541	RX J0046.0+4143	00 46 05.7	+41 43 04.0	26	2005 Dec 3
6167	RX J0046.0+4143	00 46 05.70	+41 43 04.0	24	2005 Dec 3
			Swift		
00031213001	XMMUJ003910.84+404520	00 39 23.90	+40 46 11.4	11	2008 May 30
00035337001	M31-2	00 38 56.58	+40 23 16.5	9.2	2007 Jun 6
00035425003	M31-EC-T	00 38 06.4	+40 45 24.9		2007 Jun 14
00037715002	M31-N6	00 43 57.37	+41 51 15.1	3.8	2008 Aug 21
00037722001	M31-C7	00 45 27.0	+41 47 42.2	4.5	2008 May 28
00037723002	M31-S1	00 41 35.52	+40 43 22.1	3.1	2008 Aug 21
00037724001	M31-S2	00 42 22.28	+40 53 12.5	3.5	2008 Jul 4
00031310001	OT in M31	00 42 11.42	+42 15 05.6	2.9	2008 Dec 9

Notes. Exposures of M31 examined for both old and new SSS. We give the central right ascension and declination of each image, dates of the observations and exposure time. For *XMM-Newton* data, we give the the total exposure time before intervals of high background were removed.

list. A few notable exclusions of objects previously classified as SSS are listed in Section 2.2.

2.1. Analysis of Archival X-ray Data

We did not detect any new SSS in the *ROSAT* data, and refer mostly to the work done by Supper et al. (1997), Kahabka (1999), and Greiner et al. (2004).

The largest part of the X-ray original data analysis in this work is based on *XMM-Newton*, which offers two different EPIC detectors, pn and MOS. We examined both, although the EPIC-pn sensitivity in the very soft range, and its good calibration down to an energy of 150 eV make this detector the primary instrument for SSS discovery. We used the *XMM-SAS* software v. 8.0.0. We re-extracted the EPIC-pn events file using the SAS task *epchain* with the option *badpixfind=yes* and the *epreject* task to remove detector noise at low energy, crucial when studying SSS. We analyzed images filtered in the energy range 0.15–10 keV, only single events, and the restrictive selection criterion (FLAG==0) used to avoid other artifacts in the data. We carried out spectral analysis using only the good time intervals. We only accepted sources detected at 3σ level above the background in the 0.15–1 keV range for the pn, 0.3–1.0 keV range for the MOS and ACIS-S. Since there is a considerable amount of diffuse light in M31, and the point-spread function (PSF) radius that encircles 90% of the energy is 50 arcsec, with very low S/N the choice of the background may determine whether a source is detected or not. We rejected the detection of the faintest SSS if it appears to be largely dependent on a particular choice of the background region (position and size). New SSS were searched with the criterion defined in

Orio (2006), namely $S/M \geqslant 9.3$ and $S/H \geqslant 9$, where S, M, and H are the counts above the background in $S = 0.1$–1.1 keV, $M = 1.1$–2 keV and $H = 2$–7 keV, respectively. This definition is compatible with most other definitions of SSS in the literature, even with projects done using only *Chandra*, which is not very sensitive to the softest band.

For the *Chandra* observations, we refer to by Di Stefano et al. (2004), but we also analyzed new archival data in Table 1. The *Chandra* data, pipeline processed level 2 event files, were analyzed using CIAO v. 4.0. Finally, we analyzed *Swift* data using xselect, distributed as part of the HEAsoft package.

2.2. A Catalog of All SSS in M31

Tables 2 and 3 present data on 89 SSS in M31, many already known, and some new ones. We detected only six new SSS that are not novae, to the best of our knowledge, and 14 SSS novae, whose discovery has in some cases been already announced by us or others since we started this project. All the new SSS were discovered by us in the *XMM-Newton* archival images, mostly originally proposed by W. Pietsch and the MPE group, including five pointings of the nucleus of M31 done every 2 weeks between 2007 December 27 and 2008 February 8. These exposures were about 20 ks long and undisturbed by background flares. Four of the six new SSS are extremely soft and were detected with few counts above the background. The remaining two new SSS have blackbody temperature higher than 30 eV and higher S/N, and we discuss their data in detail in Section 5.

Altogether, our SSS catalog includes 63 objects that are not known as novae in Table 2, and 26 coinciding with the positions and time of outburst of classical and recurrent novae in Table 3,

Table 2
M31 Supersoft X-ray Sources

No.	Names	R.A. (J2000.0)	Decl. (J2000.0)	Ref.	X-ray on	X-ray off	T_{eff} (eV)/ $L/10^{36}$ (erg s^{-1})	UV	Optical
1	RX J0037.4+4015	00 37 25.3	+40 15 16	[1, 2, 4]	PSPC S1	PSPC S2			
2	RX J0038.5+4014	00 38 32.1	+40 14 39	[1, 2, 4]	PSPC S1	PSPC S2, 2000 Nov	**28–38**/7.8		
						2001 Mar–Jul 2006 Jun, 2007 Jun–Jul			
3	RX J0038.6+4020 s2-26	00 38 40.6	+40 19 57.7	[1, 2, 4]	PSPC S1/S2 2000 Nov 2001 Mar–Jul 2007 Jul	... ... 2006 Jun ...	**28–38**/2.2		
4	XMMU J003910.8+404521	00 39 10.8	+40 45 20.6	[1]	2006 Jul 2007 May–Jun–Jul–Dec	... 2008 Jan–Jun	50/36	SF	Bstar
5	RX J0039.3+4047	00 39 21.4	+40 47 41	[1, 4]	PSPC S1 ...	PSPC S2 2007 Jul–Dec, 2008 Jan		SF	OB ass. A124
6	RX J0039.6+4054	00 39 38.5	+40 54 09	[1, 2, 4]	PSPC S1 ...	PSPC S2 2007 Jul, 2008 Jan		SF	
7	RX J0039.7+4030	00 39 47.5	+40 30 17	[1, 2, 4]	PSPC S1/S	... 2002 Jan 2006 Jun (2)–Jul–Dec 2007 Dec	**38**/29	SF	
8	RX J0039.8+4053	00 39 50.4	+40 53 38	[1, 4]	PSPC S1 ...	PSPC S2 2007 Dec, 2008 Jan		SF	OB ass. A122
9	RX J0040.0+4100	00 40 01.6	+41 00 51	[1, 2]	PSPC S1	2006 Jul, 2008 Jan	**52–58**/45	SF	HOT star
10	RX J0040.4+4009	00 40 26.3	+40 09 01	[1, 2, 4]	PSPC S1	2007 May–Jul–Dec			
11	RX J0040.4+4013	00 40 28.6	+40 13 44	[1, 4]	PSPC S1	PSPC S2, 2007 Dec	**28–36**/10-12		
12	PFH 75	00 40 37.7	+40 40 46.9	[6]	2001 Jan, 2002 Jan	2006 Dec			
13	RX J0040.7+4015	00 40 43.2	+40 15 18	[1, 2, 4]	PSPC S1	PSPC S2, 2007 Jun	**28–38**/27-29		
14	RX J0041.5+4040	00 41 30.2	+40 40 04	[1, 2, 4]	PSPC S1 ...	PSPC S2 2002 Jan, 2007 Jul	**31–34**/4		SF
15	XMMU J004132.9+404307	00 41 32.93	+40 43 07.61	[14]	2007 Dec	...			$V = 21.99$
16	s1-42	00 41 35.	+41 06 56.8	[5]	2000 Nov, 2001 Jul	...			SNR
17	s1-69	00 41 41.9	+41 07 16.7	[5]	2000 Nov 2001 Mar–Jun–Jul ... 2007 Nov–Dec (f)	... 2001 Oct 2005 Jan, 2006 Sep ...	<40/<10		

Table 2
(Continued)

No.	Names	R.A. (J2000.0)	Decl. (J2000.0)	Ref.	X-ray on	X-ray off	$T_{\rm eff}$ (eV)/ $L/10^{36}$ (erg s^{-1})	UV	Optical
18	s1-18	00 41 49.2	+40 56 43.8	[5]	2000 Nov, 2001 Jul 2005 Mar	... 2002 Jan			
19	RX J0041.8+4059	00 41 49.9	+40 59 21	[1, 2, 4]	PSPC S1	2000 Nov 2001 Mar–Jul, 2002 Jan 2005 Mar, 2006 Jun–Jul 2007 Jan	**29–35/65–75**		
20	RX J0041.8+4015	00 41 50.5	+40 15 55	[1, 2]	PSPC S1	...	**45/50**		
21	PFH 224	00 42 10.38	+40 51 47.4	[6]	2002 Jan	...		SF	
22	RX J0042.2+4048 oS1	00 42 16.68	+40 48 12.71	[1, 2]	PSPC S1 2001 Sep, 2002 Jan 2006 Jul, 2007 Jul(f) 2007 Dec	... ...	**39–62/10–12** 122/1.1 123/1.1	SF	OB ass. A85 $V = 19.42$
23	RX J0042.4+4044	00 42 27.6	+40 44 32	[1, 2, 4]	PSPC S1	2007 Jul	**28–38/25–35**		
24	RX J0042.6+4159	00 42 38.3	+41 59 10	[1, 2]	PSPC S1	2004 Dec	**>63/>0.7**		
25	r2-54*	00 42 38.6	+41 15 26.3	[5]	2002 Oct (f) 2005 Dec (f) 2006 Feb ...	2001 Oct 2004 Dec(3) 2005 Jan–Dec, 2006 Jan–Jun–Sep 2007 Jun–Jul–Sep–Nov(3)–Dec			
26	RX J0042.6+4043 s1-84	00 42 38.8	+40 43 17	[1, 2]	PSPC S1, 2001 Sep 2006 Jul, 2007 Dec	... ...	95,110/8		
27	r1-35*	00 42 43.0	+41 16 03.9	[5]	2001 Oct(2) ...	2004 Jul 2007 Jul–Nov(3)–Dec	130/≃10		
28	RX J0042.7+4107	00 42 44.9	+41 07 18	[1, 4]	PSPC S1	PSPC S2 2001 Oct, 2004 Jul 2005 Feb, 2006 Sep 2007 Jan–Mar–Nov(3)–Dec			
29	r2-65* PFH 336 os6	00 42 47.0	+41 14 12.4	[5]	2001 Oct	2000 Dec 2004 Dec, 2005 Jan 2006 Jun–Nov, 2007 Nov	50/20.2		
30	r2-56* oS8	00 42 50.4	+41 15 56.2	[5]	15 times (2000 Dec to 2007 Dec)	... ...			SNR
31	r2-12* oS7	00 42 52.4	+41 15 39.7	[5]	PSPC S1/S2 2001 Oct(2), 2002 Oct, 2004 Jul(3) 2007 Mar–Jun–Nov(3)–Dec 2008 Jan(3)–Feb–Mar–Jul		**65/3280** 70–75/330–2500 80/250 **66/>3**		

Table 2
(Continued)

No.	Names	R.A. (J2000.0)	Decl. (J2000.0)	Ref.	X-ray on	X-ray off	T_{eff} (eV)/ $L/10^{36}$ (erg s^{-1})	UV	Optical
32	RX J0042.9+4059	00 42 55.4	+40 59 34	[1, 2]	PSPC S1	. . .			SNR
33	r3-115* oQ12	00 43 06.9	+41 18 09.0	[5]	. . . 2001 May–Oct 2002 Jan	2000 Jun–Dec . . . 2004 Jul, Dec, 2005 Feb 2007 Jun-Nov-Dec 2008 Jan(3)-Feb-Jul			
34	PFH 401*, oS12 XMMU -J004308.5+411820	00 43 08.50	+41 18 20.7	[6]	2001 Jun–Oct	2002 Jan, 2005 Feb 2006 Jun–Dec, 2007 Nov	34/300		
35	r3-131 oS4	00 43 08.60	41 07 30.6	[7]	2000–2002	2004 Jul–Dec(2) 2005 Jan–Feb–Dec, 2006 Sep 2007 Nov(3), 2008 Feb	140/1.4		$V = 22.61$ (red star)
36	RX J0043.3+4120 r3-8 oS14 PFH430	00 43 18.89	+41 20 17.2	[1, 2]	PSPC S1 2000 Jan–Dec, 2001 Jun–Oct 2002 Jan, 2004 Dec, 2005 Feb–Dec 2006 Sep, 2007 Jan–Dec, 2008 Jul	. . . 2004 Jul 2006 Jul 2007 Mar–Nov(3)	**59–62/140** 64,73,48/30–650 ⩽25 70/73	SF	
37	XMMU- -J004319.4+411759 oS11, PFH 431	00 43 19.59	+41 17 56.9	[11]	2000 Jun	2000 Jun–Dec 2001 Jun–Oct, 2002 Jan, 2004 Jul 2005 Jan–Feb, 2006 May 2007 Jan–Nov(3)–Dec	65/295	SF	
38	XMMU- -J004329.8+410307	00 43 29.8	+41 03 09.9		2008 Jan, Feb	2006 Jun, 2007 Jul, 2008 Jul		SF SF	
39	PFH 446	00 43 25.56	+41 16 17.1	[6]	Jan 02	2004 Jul-Dec, 2005 Dec 2005 Dec, 2006 Sep 2007 Nov, 2008 Jul			
40	RX J0043.4+4118	00 43 27.9	+41 18 31	[1, 2, 7]	PSPC S1 >20 times 02-07				SNR
41	RX J0043.5+4207	00 43 35.9	+42 07 30	[1, 2, 4]	PSPC S1 1993 Jan	PSPC S2 2007 Jan	**32–39/9**		AGN
42	RX J0043.6+4126	00 43 39.2	+41 26 51	[1, 2, 7]	PSPC S1, 2000 Dec 2002 Jan	. . .			SNR
43	PFH 480	00 43 41.4	+41 34 05.3	[6]	2002 Jan	2007 Jan		SF	
44	RX J0043.7+4127	00 43 44.4	+41 27 24	[1, 2]	PSPC S1	2001 Oct, 2005 Jan–Feb 2007 Apr–Nov, 2008 Jul	**46–60/45**	SF	OB ass. A2
45	RX J0043.9+4151	00 43 54.6	+41 51 48	[1, 2]	PSPC S1	2004 Jul, 2007 Jan	**43/10–13**		
46	RX J0044.2+4026	00 44 12.2	+40 26 47	[1, 2]	PSPC S1	. . .	**>69/>1**		

Table 2
(Continued)

No.	Names	R.A. (J2000.0)	Decl. (J2000.0)	Ref.	X-ray on	X-ray off	T_{eff} (eV)/ $L/10^{36}$ (erg s^{-1})	UV	Optical
47	RX J0044.2+4117	00 44 14.0	+41 17 57	[1, 4]	PSPC S1	PSPC S2 2004 Dec, 2006 Sep–Dec 2007 Mar--Jul(3)–Dec, 2008 Jul		SF	OB ass. A32
48	XMMUJ004447.4+411847	00 44 47.35	+41 18 48.60	[14]	2006 Dec	. . .			
49	RX J0045.2+4136 XMMJ004513.9+413614	00 45 12.6	+41 36 16	[1, 2, 7]	PSPC S1 5 times(02–06)	. . .	**72–73**/5		SNR
50	RX J0045.4+4154	00 45 28.7	+41 54 06	[3,12]	1992 Jan, 1993 Jan	1991 Jul, 1992 Aug 2000 Jan–Jul, 2002 Jan 2007 Jan(2)	**72–73**/650	SF	
51	RX J0045.4+4219	00 45 29.8	+42 19 08	[1, 2]	PSPC S1	. . .	**51–59**/22		
52	RX J0045.5+4206	00 45 31.8	+42 07 06	[1, 2, 4]	PSPC S1 . . .	PSPC S2 2002 Jan, 2006 Jun, 2007 Jul	**35–40**/43	SF	OB ass. A107
53	n1-48	00 46 04.1	+41 49 42.7	[5]	2001 Nov, 2002 Jul	2005 Mar, 2006 Jun			
54	RX J0046.1+4136	00 46 10.1	+41 36 26	[1, 2]	PSPC S1	2006 Jul, 2007 Jan–Mar	> 51/>4		
55	RX J0046.2+4144	00 46 15.6	+41 44 36	[1, 2, 4]	1993 Jan	00-01? 2007 Jan–Mar	**27–38**	SF	
56	RX J0046.2+4138	00 46 17.8	+41 38 48	[1, 2, 4]	PSPC S1	PSPC S2, 2007 Jan–Mar	**29–38**/15		
57	XMMU J004644.9+412542	00 46 44.93	41 25 41.85	[14]	2007 Jan	. . .			
58	PFH 799	00 46 58.19	+41 16 56.3	[6]	2003 Feb	. . .			
59	RX J0047.4+4157	00 47 27.2	+41 57 34	[4]	PSPC S2	PSPC S1, 2007 Jan			
60	RX J0047.6+4159	00 47 42.3	+41 59 59	[4]	1992 Jan	1993 Jan			
61	RX J0047.6+4132	00 47 36.0	+41 32 08	[1, 2]	PSPC S1	. . .	>60/>6.5		
62	RX J0047.6+4205	0047 38.5	+42 05 07	[1, 2, 4]	PSPC S1	PSPC S2, 1992 Jan			
63	RX J0047.8+4135	00 47 53.9	+41 35 38	[4]	PSPC S1 . . .	PSPC S2, 1992 Jan, 2001 Jan 2001 Mar, 2007 Jan			

Notes. Catalog of SSS in M31. We list the different names starting with the first identification in the literature, and the most accurate position (*Chandra*'s when available). The sources in the central 5 arcmin of M31, that cannot be searched in our UV and ground-based optical images, are marked with an a asterisk. "(f)" indicates a remarkably lower flux level than in other detections. We give the references, alternative names, dates of X-ray detections and non-detections, effective temperature and absolute luminosity (or upper limit) for either blackbody or atmospheric fit (the atmospheric ones in boldface), with 2σ errors 20 eV for blackbody fit or 10 eV for the atmospheric fit unless otherwise noted; see the text), and finally we indicate possible counterparts in UV and optical.

References. (1) Supper et al. 1997; (2) Kahabka 1999; (3) White et al. 1995; (4) Greiner et al. 2004; (5) Di Stefano et al. 2004; (6) Pietsch et al. 2005a; (7) Orio 2006; (8) Shirey 2001; (9) Trudolyubov & Priedhorsky 2008; (10) Williams et al. 2006a; (11) Osborne et al. 2001; (12) White et al. 1995.

A CENSUS OF THE SUPERSOFT X-RAY SOURCES IN M31

Table 3
M31 Novae as Supersoft X-ray Sources

No.	Source	R.A. (J2000.0)	Decl. (J2000.0)	Ref.	Nova M31N	X-ray on	X-ray off	T_{eff} (eV)	$L/10^{36}$ (erg s^{-1})
1		00 41 40.32	+41 14 33.5		M31 N2007-02b	2008 Jan (3)			
2		00 41 49.41	+41 04 02.6		M31 N2007-08b	2007 Feb			
3	PFH 191	00 41 54.26	+41 07 23.9	[1, 2, 3, 10]	2001-10f	2002 Jan ...	2004 Dec (f), 2005 Jan 2006 Sep, 2007 Nov(3)–Dec	54, 51	785, 180
4		00 41 54.94	+41 09 47.4		2007-12d	2007 Dec			
5	XMMU- -J004159.1+404430.3	00 41 59.13	+40 44 30.3		2005-01b	2006 Jul	2007 Dec, 2008 Jan-Feb	⩽30	⩽20
6	asrc165*	00 42 22.36	+41 13 45.12	[2]	2004-06a	... 2005 Mar–Dec	2001 Oct, 2004 Jul 2007 Mar–Nov(3)–Dec, 2008 Jul		
7		00 42 30.38	+41 35 55.7		2008-02a	Dec 07	Jan 08		
8		00 42 33.14	+41 00 25.9		2007-06b	2008 Jan, Feb			
9	PFH 313*	00 42 42.14	+41 12 18.2	[1, 2, 3, 4]	1994-09a	2001 Oct, 2002 Jan ...	2005 Feb, 2004 Sep 2007 Apr–Nov(3)–Dec, 2008 Jul		
10	r2-60*	00 42 43.95	+41 17 55.7	[1, 2, 4, 5]	2000-07a	2001 Jan, 2002 Oct, 2004 Dec 2005 Dec, 2007 Nov	2000 Jun	20 ± 10 <60	<5 <10
11		00 42 44.45	+41 16 10.5		2004-09b	2007 Dec, 2008 Jan (2)	2004 Jul		
12	asrc229	00 42 46.11	+40 53 34.54	[6]	1999-08d	2001 Jul (2)	2004 Jul, 2007 Jun, 2008 Jul		
13	r2-61*	00 42 47.3	+41 15 07.2	[2, 5]	2000-08a	2000 Dec, 2001 Oct(2) 2002 Jan–Jun	2004 Jul–Dec 2005 Jan–Feb–Dec 2006 Sep, 2007 Jun–Nov(3),Dec 2008 Jul	⩽5	
14	S08 886*	00 42 49.74	41 16 33.2	[1, 3]	1999-10a	2004 Jul–Dec, 2005 Jan–Feb	2001 Oct		
15	XMMU -J004272.7+411428*	00 42 52.71	41 14 27.84	[1, 3, 7, 8]	2005-02a	2006 Jul	...	40	140
16	PFH 359* oS15	00 42 55.23	+41 20 47.0	[1, 3, 7, 8]	1996-08b 1925-01a	2001 Oct, 2002 Jan 2005 Jan–Feb–Dec, 2006 Dec 2007 Nov(3), 2007 Dec	2000 Jun–Dec	⩽55 80 ± 20	⩽39 ⩽155

Table 3
(Continued)

No.	Source	R.A. (J2000.0)	Decl. (J2000.0)	Ref.	Nova M31N	X-ray on	X-ray off	$T_{\rm eff}$ (eV)	$L/10^{36}$ (erg s^{-1})
17	r2-63* PFH 369	00 42 59.3	+41 16 42.8	[1, 4, 5, 7]	1995-11c ...	2001 Jun–Oct, 2002 Jan–Oct 2000 Jun–Oct, 2008 Jan–Jul 2004 Jul, 2005 Dec	2007 Jun–Nov(3), 2008 Jul	34(J02)	365
18		00 43 04.14	+41 15 54.2		2007-11c	2007 Dec, 2008 Jan	2008 Jan		
19		00 43 07.40	+41 18 04.3		2004-11b		2008 Jan		
20		00 43 19.98	+41 13 46.4		2007-12b	2007 Dec, 2008 Jan(3), 2008 Feb	2008 Jul	**76**	**300**
21		00 43 27.18	+41 10 03.3		2008-06c	2007 Dec	2008 Jan		
22		00 43 29.53	+41 17 13.8		2007 10-b	2007 Dec, 2008 Jan(3),Feb			
23	RX J0044.0+4118	00 44 04.8	+41 18 20	[9]	1990-09a	PSPC-S1	2005 Jan, 2006 Sep-Dec 2007 Mar–Nov(3)–Dec, 2008 Jul	**32–39**	33
24	PFH 543, CXOU--J004414.3+412205	00 44 14.3	+41 22 05	[2, 8, 11, 12]	2001-11a	2002 Jan(2)	2006 Dec, 2008 Jul		
25	asrc216	00 44 32.58	+41 25 21.25	[6]	2001-10b	2002 Jan–Nov	2006 Dec, 2007 Jan, 2008 Jul		
26	XMMU--J004540.5+413806	00 45 40.50	+41 38 06.46		2005-01c	2008 Jan (2), 2008 Feb	...	≤30 eV	≤40

Notes.
references. (1) Pietsch et al. 2005a; (2) Pietsch et al. 2007; (3) Stiele et al. 2008; (4) Kaaret 2002; (5) Di Stefano et al. 2004; (6) Nelson et al. 2008; (7) Orio 2006; (8) Pietsch et al. 2005b; (9) Nedialkov et al. 2002; (10) Smirnova & Alksnis 2006; (11) Trudolyubov et al. 2005; (12) Garcia et al. 2002.

with the same basic notations used in Table 2. We draw on the results of the studies mentioned in Section 1 and on published reports of transient objects (Nedialkov et al. 2002; Pietsch et al. 2005a, 2007; Orio 2006; Nelson et al. 2008, and circulars referenced in the tables). The estimated *absorbed* fluxes of all SSS in the table are in the range from a few times 10^{-14} to a few 10^{-13} erg s^{-1} cm^{-2}. In the table, we also include an estimate of the absolute luminosity at M31 distance only if a spectral fit was possible, allowing us to estimate the column density N(H). For the *ROSAT* sources, spectral atmospheric temperatures were estimated by Kahabka but we added our own estimate of the bolometric luminosity with the parameters given by this author (see below).

Only the two sources r2-12 and Nova-M31 2007-12b exceed a few times 10^{38} erg s^{-1} at a distance of 780 kpc. Most *Chandra* and *XMM-Newton* detections are several sigma above the background, whereas the *ROSAT* detections were obtained by stacking several different images, often reaching only a 3σ level. Assuming N(H)$\leqslant 10^{21}$ cm^{-2}, all SSS in the tables are consistent with $L_x \geqslant 10^{36}$ erg s^{-1} at M31 distance.

Only a handful of previously reported SSS were not included in Tables 2 and 3. Source 518 of the catalog of Pietsch et al. (2005a), and the candidate counterparts of Novae 1997 08-b and 2000-06a (Pietsch et al. 2005a) are uncertain detections with extremely low S/N. Among the SSS detected with *Chandra* we excluded r3-122 (the second SSS in Table 2 of Orio 2006), identified with a foreground object at $V = 13.36$ and at < 2; r1-25, a border-line SSS in some observations, but generally variable in flux and spectrum (see Di Stefano et al. 2004 and B. Patel et al. 2010, in preparation); and r2-66 (SSS number 13 in Table 2 of Orio 2006), an SNR that is more correctly classified as a "Quasi-Soft" source by Di Stefano et al. (2004).

In addition to the novae in Table 3, about the same number of X-ray sources observed with the *Chandra* HRC-I camera, which does not offer spectral resolution but is very sensitive at low energies, coincide with the position of classical or recurrent novae (Pietsch et al. 2005a, 2007; Henze et al. 2009a). Lacking spectroscopic confirmation both in the optical and in the X-rays, most of the HRC-I sample may be contaminated by black hole and other transients, for instance WZ Sge-like outbursts (thought to be exceptionally large disk instabilities) in the foreground.

Table 2 includes, for statistics and comparisons, six known SSS that have already identified as SNR in optical narrow-band imaging surveys. On average, the SNRs are quite harder than the other SSS in Table 2 for which there is sufficient signal to obtain a broadband spectrum. They are also harder than typical novae, and are border-line "Quasi-Soft-Sources" (QSS) as defined by Di Stefano et al. (2004). An AGN-like optical spectrum has been observed only for the likely counterpart one SSS no. 42 in Table 2 with the Subaru 8 m telescope (out of six SSS selected for that study; J. Greiner & R. Schwarz 2009, private communication).

Given the large number of new images we used in this study, six new SSS not known as novae may appear few compared with the 16 new SSS detected in the first *ROSAT* survey of M31. This is partly because the *ROSAT* observations covered a much larger area of the galaxy than *Chandra* and *XMM-Newton*, almost 6 deg^2. The new *XMM-Newton* and *Chandra* pointings often revisited the same location in M31, and the observations do not extend to as large galactocentric radii as the *ROSAT* ones. However, in the same exposures between 2004 and 2008 as many as 14 other new SSS were detected that coincide with novae in position and time, confirming that the largest class of
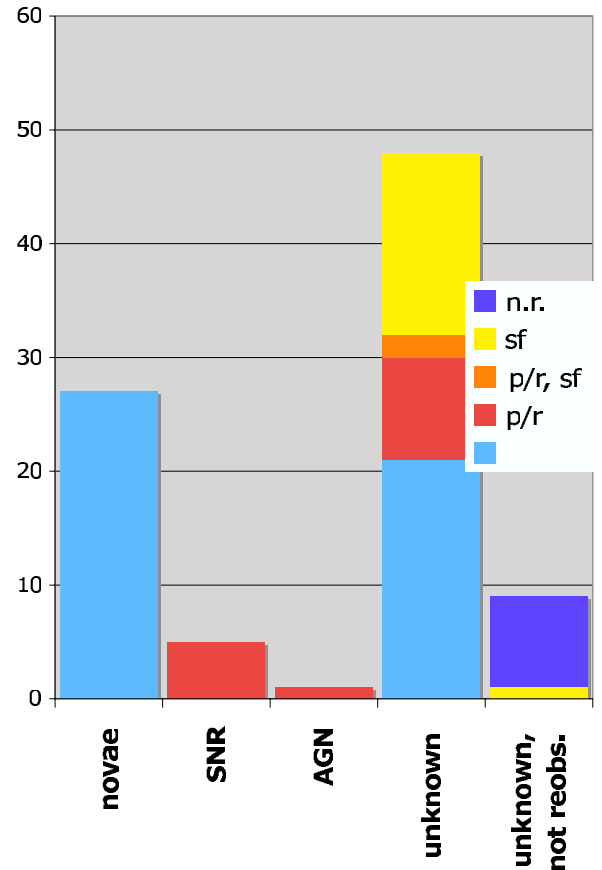
Figure 1. Distribution of M31 SSS known to be novae, SNR, AGN, not identified but at least observed again in X-rays, or not identified but not re-observed in X-rays. The red color indicates persistent or recurrent sources, the yellow indicates SSS coinciding with star formation region or B stars, and the intersection of the two groups is in orange. The "unknown, and not re-observed" SSS are represented in darker blue.

(A color version of this figure is available in the online journal.)

SSS is indeed post-outburst novae (Pietsch et al. 2005a). Nova monitoring in M31 has been much more intensive and complete between 2004 and 2008 than in previous years; therefore it is difficult to assess how many of the *ROSAT* SSS may have been novae. In the next session, we show that the duration of most *ROSAT* SSS was typical of novae, that may have eluded observations from the ground.

2.3. Long-term X-ray Behavior

In Figure 1, we show the basic classification of the M31 SSS in known classes of objects, and in persistent/recurrent and transient sources. Ten SSS that were not re-observed are grouped in the last bin of the histogram, colored in darker blue. Greiner et al. (2004) already found that many SSS in M31 are not steady sources. In Tables 2 and 3, we list the dates on which the sources were observed in X-rays, whether they were detected or not, and in the few cases in which a spectral fit is possible, we include a blackbody or even an atmospheric temperature, and the absolute luminosity for that temperature. This has been possible only for few SSS observed with either *XMM-Newton* or *Chandra*. We do include some spectral fits attempted for the *ROSAT* SSS by Kahabka (1999) with a WD atmospheric model (a 2σ range of temperature) but we caution that they were obtained with N(H)$> 8 \times 10^{20}$ cm^{-2}, and in some cases the author estimates even a few times 10^{21} cm^{-2}, largely exceeding

the column density between us and M31. These fits are very uncertain, mainly because the *ROSAT* detection are based on stacked images and on few counts, The luminosity is not given by the author, and a duplication of the result is not possible without knowing what set of abundances was assumed for the fit. However, we know that the hot WD atmospheric luminosity is about 1/10th of the equivalent blackbody luminosity for the models used by Heise et al. (1994) and by Kahabka (1999) and other atmospheric models used by us in previous papers (note that Heise et al. 1994 assume a distance to M31 of only 650 kpc whereas we assumed 780 kpc). Therefore, for all fits by Kahabka (1999) we also give in Table 1, as an approximate estimate, 1/10th of the equivalent blackbody luminosity for temperature, N(H) and count rate indicated by the author for each object. We did not include the upper limits on the temperature of other SSS from the same paper, because they are not very constraining, given an a priori assumption of very high N(H).

In Table 1, we claim a non-detection if the upper limits on the count rates are lower than all the previously measured count rates. This may only mean that the effective temperature of the object decreased, while the X-ray flux is beyond the detection threshold. In fact, the tables show that the persistent or recurrent sources are those at high temperatures, generally above 60 eV. It is thus possible some apparently transient SSS may have not been detected again only because of temperature fluctuations in the EUV regime, but we show in the next section that the lack of UV counterparts in many cases seems to rule out this possibility (Section 3).

We converted the count rates of different detectors with PIMMS and a blackbody model with a temperature that was either appropriate for each source, or we set it to 50 eV where no broadband spectrum could be obtained (this is the case of all the *ROSAT* sources). In a few cases of detections with remarkably lower count rate, we added "(f)" for *faint*. The information in the tables shows the duty cycle of all the known SSS and their long-term variability timescales. A more detailed account on the evolution of the best observed sources will be presented in a forthcoming paper (M. Orio et al. 2010, in preparation).

Figure 1 is a graphic representation of the statistics. Out of 63 sources in Table 2, 51 have been observed again in X-rays over timescales of several years, yet only 11 SSS that are not classified as SNR appear to be persistent or recurring sources (i.e., they were not observed to "turn off" completely like novae do). Only three sources were always detected when re-observed (RX J0042.2+4048, RX J0042.6+4043 or s1-84, and r2-12), although we note that r2-12, the brightest M31 source, is variable (Di Stefano et al. 2004; Orio 2006; Trudolyubov & Priedhorsky 2008). Seven other SSS appear to be recurrent or variable, and have been detected sporadically (RX J0038.6+4020 or s1-26, RX J0043.3+4120 or r3-8, r3-131, RX J0045.4+4154, r2-54, s1-28, PFH 401). The upper limits on the non-detections are not always sufficient to assess the variability timescale. Moreover, source confusion is a problem for SSS near the core in the *XMM-Newton* exposures, so observation of the most central sources is not possible with this satellite.

Greiner et al. (2004) noted a large difference in the number of SSS detections between the first and second *ROSAT* PSPC surveys and attributed it to the fact that they were achieved by stacking images taken at different intervals times: within days in the first survey, but over many months in the second survey. These authors concluded that SSS must be "on" for only timescales of days. With more data we can now see, however, that a large number of SSS (both known and not known as novae)

are "on" for years before turn-off. Thus, although we do confirm the basic finding of Greiner et al. (2004), that the majority of all SSS discovered in M31 are transient, the pattern that is beginning to emerge is consistent with classical and recurrent novae.

Figure 1 also indicates 17 still unidentified sources (in yellow or in orange if they overlap with the "red" persistent sources) that overlap with the star-forming region and/or with very massive stars (B or O spectral type). Seventeen out of a sample of 49 sources residing outside the crowded core (the one in the core cannot be resolved except with *Chandra* and *Hubble Space Telescope* (*HST*) is a very significant number, representing 35% of the total. Only one SSS of this group was not observed again, yet only two have been repeatedly observed: a persistent source (see Section 6.1) and a recurrent SSS flare after a year (see White et al. 1995). These SSS appear in the the orange stripe in Figure 1, as intersection with the "red" sources. We will explore the meaning of this discovery in the next sections.

3. SSS IN OPTICAL AND ULTRAVIOLET IMAGES

Paczyński (1971), Fujimoto (1982), and Nomoto et al. (2007), among other authors, have predicted that WDs burning hydrogen in an accreted shell with a high-mass accretion rate may have thin atmospheres with an effective temperature in the range of 10^5–10^6 K, so the peak of their spectral energy distribution is in the extreme ultraviolet (EUV) or soft X-rays (see Figure 2, upper panel). This has been confirmed observationally for several novae in outburst (e.g., Balman et al. 1998; Orio et al. 2001; Nelson et al. 2008). Such high temperatures place all optical and UV filters on the Rayleigh–Jeans tail of the blackbody distribution. SSS are 10 to 100 times brighter in UV than in optical, depending on the effective wavelength and the degree of extinction toward the source (again this is confirmed observationally by comparing optical spectra of SSS in the Magellanic Clouds with those obtained using *IUE*, *FUSE,* and *HST*). The *V*-band magnitudes of LMC SSS range from ∼21.7 (RX J0439.8−6809) to ∼16.7 (RX J0513.9−6951 in its "high" optical state; see also Šimon 2003). Thus, at the distance of M31 (780 kpc; Sparke & Gallagher 2007) these sources would be at magnitude $28 \lesssim m_V \lesssim 23$.

Several MC and Galactic SSS are known to be transient or recurrent in soft X-rays. For some systems, e.g., CAL 83 (Greiner & Di Stefano 2002) and RX J0513.9−6951 (Reinsch et al. 2000), an anti-correlation between X-ray and UV luminosity has been discovered. The sources brighten in the UV as they fade in X-rays. This behavior has been interpreted as an expansion of the accreted shell of the WD in response to a change in accretion rate from the secondary. The photosphere cools to an effective temperature $T_{\mathrm{eff}} \leqslant 100,000$ K, shifting the peak of the emission to the EUV or UV, as Figure 2 clearly shows. Systems that are no longer bright in X-rays may still be detected in the UV range if they are undergoing such behavior. Another significant source of UV emission is the irradiated accretion disk, with a UV flux 10–50 times larger than the optical flux (a 2.5–4 mag difference). At the distance of the MC, and sometimes even at the distance of M31, the disk may be sufficiently luminous to be detected with *GALEX*, in addition to the UV luminosity due to nuclear burning.

The distribution of our SSS catalog in M31 is shown on an optical image obtained with the 90 cm Asiago telescope (see Figure 3, where the astrometric solution was a courtesy of W.
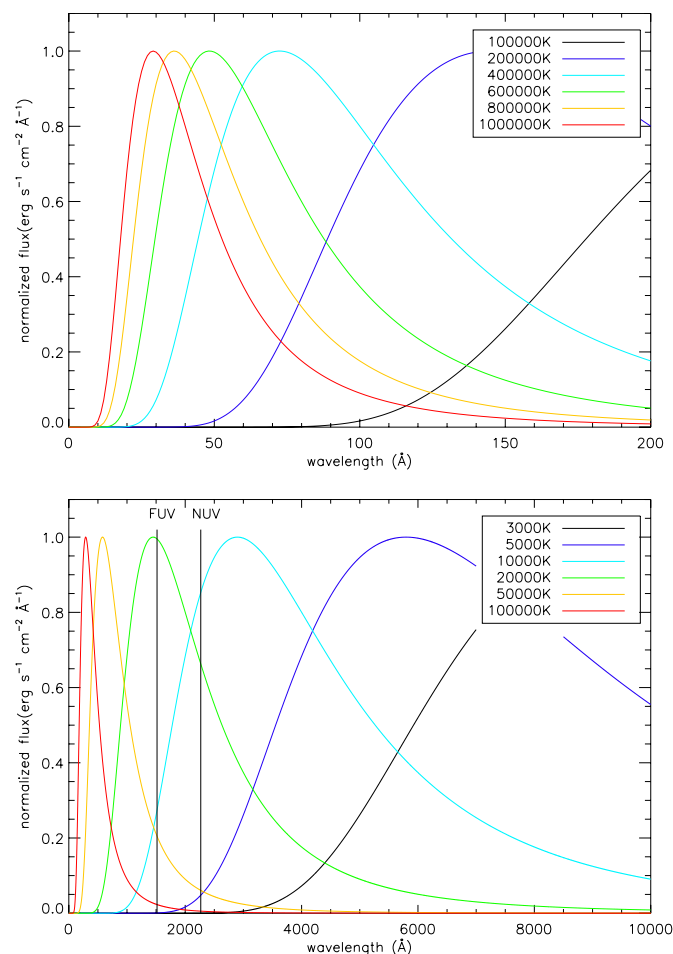
Figure 2. Normalized fluxes for blackbodies in the wavelength region 1–200 Å (including the effective temperatures in the 10^5–10^6 K temperature range expected for shell burning WD, upper panel), and in the wavelength range up to 10000 Å (lower panel). The vertical lines indicate the wavelengths of the *GALEX* filter bandpasses.

(A color version of this figure is available in the online journal.)

Pietsch and the MPE group). The major obstacle in identifying multi-wavelength counterparts of SSS observed with *ROSAT* (and to a lesser extent *XMM-Newton*) is the large number of objects located in the spatial error circle, which at the 2σ accuracy level has a radius of 10–15 arcsec for *ROSAT*, and ~3 arcsec for *XMM-Newton*. Only images obtained with *Chandra* provide a spatial position error of the order of an arcsec or less. Note that a non-negligible number of SSS (in yellow in Figure 1) appear to be in, or superimposed on, the spiral arms of M31, unlike binary SSS containing small mass secondaries. We will discuss this point in detail below.

We made use of public UV images of M31 obtained with *GALEX*, *Swift,* and *XMM-Newton*, of the Local Group Survey (LGS) optical images and catalog of M31 (Massey et al. 2006), and of deep images of selected SSS obtained by us using the WIYN 3.5 m telescope. In tandem, UV and optical data allow us to characterize the possible counterparts, to look for variability (which may be evidence of binarity), and to investigate the properties of the environments where SSS are located. Due to difficulties in resolving sources in the bulge of M31 at both optical and UV wavelengths (either due to diffuse light or low spatial resolution) we included in our search only the SSS outside the inner 5 arcmin of the galaxy—a total of 55 sources in Table 2, 48 of which were not identified. These are also
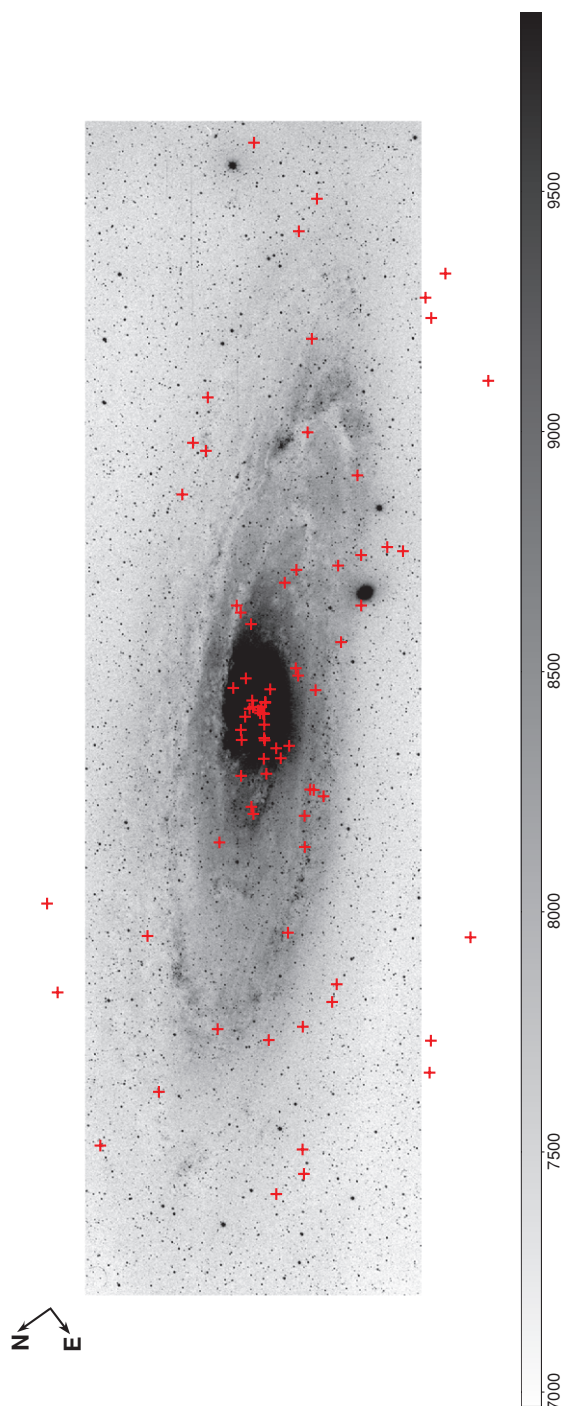
Figure 3. Image of M31 with positions of SSS indicated by red crosses. SSS identified as foreground stars have been removed.

(A color version of this figure is available in the online journal.)

the sources that can be resolved with *XMM-Newton*. We also embarked in a separate project with collaborators, looking for counterparts of the eight other SSS in the core of M31 in *HST* images (Patel et al. 2008; B. Patel et al. 2010, in preparation).

3.1. UV and Optical Images

GALEX is a small explorer class NASA mission (for a full description of the observatory, see Martin et al. 2003). The telescope has a 0.5 m modified Ritchey-Chretien, aspheric corrected primary mirror with a 1°.2 field of view (FOV), and two

Table 4
UV Images of SSS in M31

Obs ID	R.A. (deg)	Decl. (deg)	Date	Exposure Time (s)
		GALEX Nearby Galaxy Survey		
NGA_M31_F1	10.64656	+41.25435	2003 Sep 5 20:21:05	1446
NGA_M31_F2[a]	9.94335	+40.59946	2003 Sep 5 21:58:25	4509
NGA_M31_F3	11.24993	+41.86491	2003 Sep 5 05:32:06	1912
NGA_M31_MOS0	10.17611	+40.83596	2004 Sep 27 04:51:04	1631
NGA_M31_MOS3	11.39647	+40.51601	2003 Oct 19 03:24:32	1361
NGA_M31_MOS4	11.19267	+41.53695	2003 Oct 9 06:39:53	2570
NGA_M31_MOS7	10.89216	+42.56733	2003 Oct 9 03:22:34	2760
NGA_M31_MOS8	12.18019	+42.03367	2003 Oct 9 09:57:12	1027
NGA_M31_MOS12	10.34112	+40.36656	2003 Oct 8 12:34:39	3029
NGA_M31_MOS17	10.59593	+41.98868	2004 Nov 14 08:27:09	6812
NGA_M31_MOS18	11.40181	+42.37063	2004 Sep 27 08:08:20	3255
		GALEX Deep Imaging Survey		
PS_M31_MOS00	10.68107	+41.27566	2007 Sep 18 06:02:40	3760
PS_M31_MOS01	11.45021	+40.40104	2007 Sep 19 03:24:13	2657
PS_M31_MOS02	10.85485	+40.25038	2007 Sep 19 05:02:47	3033
PS_M31_MOS03	9.95709	+40.35847	2007 Sep 15 09:02:45	1182
PS_M31_MOS04	9.38731	+40.88089	2007 Sep 15 04:07:01	1486
PS_M31_MOS07	10.59543	+42.34723	2007 Sep 16 08:02:28	4666
PS_M31_MOS08	11.34961	+42.19303	2007 Sep 17 08:41:08	2765
PS_M31_MOS09	12.17314	+42.03743	2007 Sep 17 21:49:46	2261
PS_M31_MOS10	11.18783	+41.39165	2007 Sep 18 20:49:53	1242
		GALEX All Sky Survey		
AIS_38	9.68836	+41.02086	2006 Nov 7 01:32:58	104
		Swift UVOT		
00031213001	00 39 23.90	+40 46 11.4	2008 May 23 03:48:01	3713 (UVM2)
				2928 (UVW1)
				3833 (UVW2)
00037710002	00 39 48.49	+40 58 13.3	2008 Jul 21 14:24:01	1636 (UVM2)
				1507 (UVW1)
				1636 (UVW2)
00037723002	00 41 35.52	+40 43 22.1	2008 Aug 21 18:59:01	904 (UVW1)
				1078 (UVW2)
00037724001	00 42 22.28	+40 53 12.5	2008 Jul 4 14:30:37	1117 (UVM2)
				1053 (UVW1)
				1303 (UVW2)
00035336001	00 42 48.56	+41 15 29.6	2007 Jun 1 16:37:00	5098 (U)
				13034 (UVW2)
00031255001	00 42 55.51	+41 17 21.2	2008 Aug 21 07:20:01	1879 (UVW1)
				2036 (UVW2)
00037720002	00 43 42.65	+41 27 19.7	2008 May 28 20:15:01	965 (UVM2)
				966 (UVW1)
				965 (UVW2)
00037726002	00 44 00.77	+41 13 44.0	2008 Jul 22 01:39:01	1446 (UVW1)
				1097 (UVW2)
00037722001	00 45 27.02	+41 47 42.2	2008 May 28 01:06:01	1504 (UVM2)
				1379 (UVW1)
				1504 (UVW2)

Notes. R.A. and decl. are in J2000.0 coordinates. The date given in Column 4 is the start time of the first subvisit of each tile.
[a] FUV only.

microchannel plate detectors are used to carry out simultaneous imaging in two bands; far ultraviolet (FUV, 1350–1800 Å) and near ultraviolet (NUV, 1800–2800 Å). A low resolution ($R = 150$–300) grism spectroscopy is also available. For the NUV band, the angular resolution is $5''$ FWHM, with an effective area of 44 cm^2, in the FUV band, the spatial resolution is $3''.3$ FWHM, but the effective area is smaller (25 cm^2). These FWHMs correspond to 19 and 12.5 pc at the distance of Andromeda. M31 was initially surveyed by *GALEX* at two different epochs during the Nearby Galaxies Survey (NGS; Bianchi et al. 2003; Thilker et al. 2005) in a series of 26 "tiles" between 2003 September and 2005 September. Subsequently, M31 has been re-imaged as part of the *GALEX* Deep Imaging Survey (DIS), with 11 tiles obtained in 2007 September. M31 also falls on one of the All Sky Survey (AIS) tiles, although the galaxy is only partially imaged and the exposure time is very short. All the regions of M31 observed with X-ray satellites have been covered with *GALEX*. A summary of the observations is in Table 4. We examined the *GALEX* intensity map images corrected for the normalized relative response of the detector.

Due to the nature of the optics on board *GALEX*, the PSF becomes distorted within the outer $0°1$ of each image. Therefore, we confined our photometry to sources lying outside the central 5 arcmin circle and within the inner $1°1$ of the FOV. We performed aperture photometry using the APPHOT package in IRAF,[7] with a 6 pixel aperture for the photometry (see Rey et al. 2005), and we calculated an aperture correction examining isolated stars. We converted the observed count rates to fluxes and AB magnitudes using conversion factors outlined in the *GALEX* observers handbook. A further conversion to the vega magnitude system in the *GALEX* bandpass, for comparison with theoretical isochrones, was done by subtracting 2.224 (1.699) from the AB magnitudes in the FUV (NUV) bands (L. Bianchi, 2008, private communication).

The UV Optical Telescope (UVOT) instrument on *Swift* and the Optical Monitor (OM) on board *XMM-Newton* share a common design, using a microchannel plate intensified CCD detector with a $17'$ by $17'$ FOV and sensitivity from 1700 to $6500\,\text{Å}$ in six filters (for a full description see e.g., Mason et al. 2005 (OM); Roming et al. 2005 (UVOT)). Although observations of M31 with these instruments do not cover as large an area as the *GALEX* surveys, or reach as far into the FUV, they do achieve higher spatial resolution ($2''$ versus $3''.3$) and can therefore complement the *GALEX* observations, particularly in crowded regions. The filters are narrow and the filter's central wavelengths are $2600\,\text{Å}$ for the UVW1, $2240\,\text{Å}$ for the UVM1, $1928\,\text{Å}$ for the UVW2. Because the FOV of these telescopes is smaller than their X-ray counterparts, they do not always image the location of any SSS detected in that observation. We examined all *Swift* UVOT images in the HEASARC archive with exposure times longer than 2000 s (see Table 4 for details). We reduced and analyzed the images using the *Swift* specific tasks in xselect V2.4a distributed as part of the HEASOFT package. Individual exposures from each observation were combined to produce a single, deep image per filter using the *uvotimsum* task. Again, where possible, we performed photometry of potential counterparts using the *uvotsource* task and a $3''$ aperture as recommended in the UVOT users guide. For the *XMM* OM data, we followed the procedures outlined in the *XMM-Newton* ABC analysis guide for our photometric measurements.

For the LGS, the entire disk of M31 was imaged with the KPNO 4 m telescope and the MOSAIC imager, an $8K \times 8K$ CCD array providing a $36'$ by $36'$ FOV, at optical wavelengths with *U*, *B*, *V*, *R*, and *I* broadband filters as well as Hα, O III, and S II narrow-band filters. Broadband photometry and colors are available as part of the data release. The photometry is accurate at a 1% level at 21st magnitude, and at a <10% level at 23rd magnitude. Sources are included in the catalog if they are detected in all three of the *B*, *V*, and *R* filters at 3σ level above the background. This survey complements the large area of M31 covered by the *GALEX* survey, and covers all but five of the sources included in our search. The *U* band images are particularly useful, as light in this band most closely traces the UV emission, and allows the source(s) of UV light to be identified.

Finally, we used the WIYN telescope for deep optical imaging of the fields of three sources in 2004, 2005, and 2006. Most images were obtained using the MiniMo camera, a CCD mosaic made up of four 1024 by 4096 CCDs providing a $9'$ by $9'$ FOV (Saha et al. 2000). An additional set of images was obtained on 2004 September 27 with the OPTIC detector, a different CCD mosaic. The images were registered to the coordinates (WCS) of the LGS, obtaining an agreement in positions within $0''.05$. The magnitudes of objects in the WIYN images were absolutely calibrated using the LGS data.

3.2. The Extinction Toward the SSS

In order to evaluate the effects of interstellar reddening on the colors of any potential counterparts, we estimated the extinction toward each SSS using H I radio maps of M31 created by Unwin (1980). The maps were obtained using the Half Mile telescope and have a spatial resolution of 48 arcsec × 72 arcsec, and trace the internal H I content of M31. These are the highest resolution maps publicly available at the time of writing. We converted from integrated H I brightness (in units of K km s^{-1}) to column density using the following relationship

$$N(\text{H}) = 1.823 \times 10^{18} \int T_b \, dv \ \text{cm}^{-2}. \quad (1)$$

This H I column density is through the entire disk of M31. Working under the assumption that the majority of our sources are near the midplane of the disk, we then converted to $E(B-V)$ using half the observed column density as follows:

$$E(B - V) = \frac{0.5N(\text{H})}{5.58 \times 10^{21}}. \quad (2)$$

Once a value of $E(B - V)$ was obtained, we used the reddening law of Cardelli et al. (1989) to calculate the value of A_λ, the extinction in magnitudes at wavelength λ. Using the effective wavelengths of the two *GALEX* bands, this law yields the following relationships:

$$A_{\text{NUV}} = 8.9 \times E(B - V) \quad (3)$$

$$A_{\text{FUV}} = 8.16 \times E(B - V). \quad (4)$$

Note that throughout the paper we will plot the observed magnitudes, with no extinction correction. It is in fact possible that all of the fainter, lower temperature SSS are not at the midplane, but rather in the part of the Galaxy facing us. We introduced corrections for absorption only to prove that the absorption is not an important bias effecting in our conclusions.

4. UV AND OPTICAL COUNTERPARTS

Figure 3 shows that many SSS lie on the spiral arms or near regions of active star formation, well traced by *GALEX*. Novae and low-mass X-ray binaries are not normally associated with the youngest stellar populations. To match the *GALEX* and *Swift* positions with the SSS X-ray positions, we assumed the 2σ positional error of each source, and added in quadrature an additional arcsecond to account for systematic offsets in the astrometry of *GALEX* and the original reference frame of the source in question. *GALEX* provided the most useful data set. The *GALEX* survey of M31 covered the most extended area in this galaxy at UV wavelengths. Moreover, the FUV filter of *GALEX* extends to shorter wavelengths than the *Swift* UVW2 filter, allowing us to probe the temperature region around and slightly below 100,000 K much better. Evolutionary tracks are also available in the bandpass of the *GALEX* filters (Girardi et al. 2002).

---

[7] IRAF is distributed by the National Optical Astronomy Observatory, which is operated by the Association of Universities for Research in Astronomy, Inc., under cooperative agreement with the National Science Foundation.

Many SSS are peripheral, they were detected only with *ROSAT* and have multiple counterparts, often unresolved. Table 5 shows the optical and UV photometric measurements for few possible counterparts of SSS that can be well resolved spatially. The table reports also the "Q" index, based on optical colors only, and described in the next section. This value can be close to −1 for both O–B stars, and for H-burning WDs. Optical color indices of several Galactic and LMC SSS are given by Šimon (2003) and we find that the Q-values of those SSS are generally $\leqslant -0.5$.

UV color indices allow us to distinguish a hot, accreting, and H-burning WD from a young, massive star. Revisiting Figure 2, the lower panel shows normalized fluxes for blackbodies with effective temperatures between 3000 and 100,000 K. We have marked the effective wavelength of the two *GALEX* bands. Assuming constant luminosity, the stars whose luminosity peaks in the UV have effective temperature in the range 10,000–20,000, of spectral class B, which are the most common objects observed with *GALEX* in M31. However, having higher bolometric luminosity by 2–3 orders of magnitude, the Raleigh–Jeans tail of a shell H-burning WD can be as UV luminous as a B-type supergiant. Only the slope of the continuum, hence the UV color indices, indicates that we are dealing with very different objects. Blackbodies with $T_{\rm eff} > 100,000$ K have a constant FUV−NUV color −0.5, since both *GALEX* bands lie on the Rayleigh–Jeans tail of the distribution. Moreover, the spectral energy distribution of hot WD differs from a blackbody because of optical depth effects, that enhances emission at shorter wavelengths making the FUV−NUV color even more negative. Generally, the detection of a UV counterpart with such negative value of FUV−NUV indicates the presence of a hot, compact object.

The Padova isochrones (Girardi et al. 2002) are also calibrated in *GALEX* magnitudes. To find out whether the UV object is also the source of the supersoft X-rays, in Figure 4 we show the UV color–magnitude diagram (CMD) of the only four objects for which we could measure UV magnitudes with *GALEX*. The isochrones in the figure are for $Z = 0.019$ stars of ages 10^7–10^9 years, for $E(B - V) = 0$ and $E(B - V) = 0.5$ (the range of reddening of the SSS catalog sources). Three of the sources have magnitudes and color indices that are typical of young, massive stars. In the next section, we show that follow-up spectroscopy of the candidate counterpart of RX J0042.2+4048 confirms this result. The candidate counterpart of only one of the four objects, RX J0040.0+4100, does not fall on any of the isochrones, but is obviously a much hotter object. The field of this source was observed again with *XMM-Newton* in 2006 and 2008; however in 2006 the *ROSAT* position was very close to a row of bad pixels in the chip, and in 2008 it was very close to the junction between chips. Given the large uncertainty in the *ROSAT* position, under these circumstances it seems that the *XMM-Newton* observations were not conclusive regarding the possible "turn off" of this SSS. Certainly at the time of the *GALEX* observations, it was still extremely hot.

We cannot draw any clear-cut conclusion for the objects in Table 5 that were observed only for *Swift*, however we note that the third possible counterpart of RXJ 0043.7+4127 also seems to be a hotter object than a B or O star.

5. COLOR–MAGNITUDE DIAGRAMS OF THE SSS FIELDS

The LGS images (Massey et al. 2006) have a much higher spatial resolution than the *GALEX* ones. In addition to using
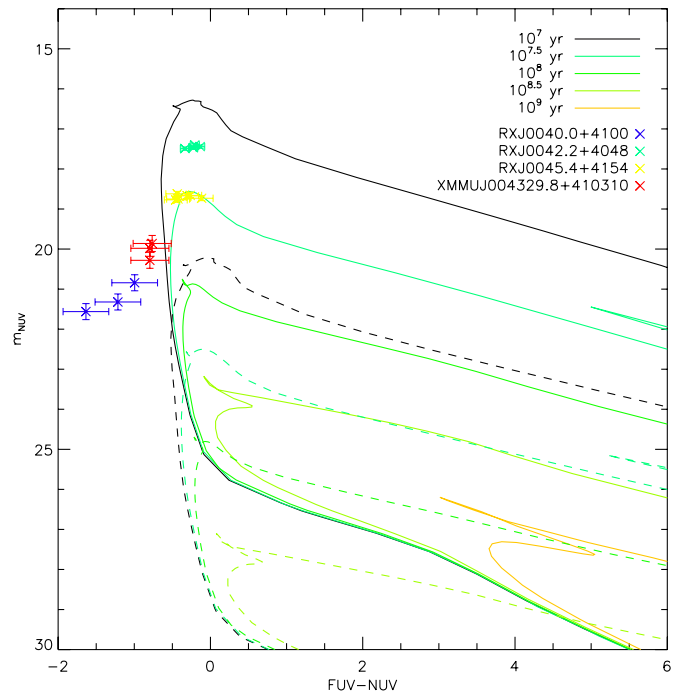
Figure 4. UV CMD for UV detected SSS. Plotted are Padova isochrones in the *GALEX* filter bandpasses, for zero extinction (solid line) and $E(B - V) = 0.5$ (dashed line), and for ages from 10^7–10^9 years. Note that these magnitudes are in the vega system (see body of text for conversion factors from AB to vega system).

(A color version of this figure is available in the online journal.)

them to pinpoint the individual sources likely to be responsible for the UV emission, we found the LGS extremely useful for investigating the environmental conditions of each SSS, and to compare the stellar populations near the SSS with UV counterparts to those SSS with no UV sources within the X-ray error circle. For each source we extracted all stars within the 2σ X-ray position error circle from the local group survey. We then created CMDs for each of the four colors included in the LGS data release—$B - V$, $U - B$, $V - R$, and $R - I$ are presented in Figure 5. The black points represent objects near the set of SSS with UV counterparts, the red points represent objects near SSS without bright UV counterparts. We overplot the Padova isochrones for $Z = 0.019$ stars of ages 7–10 Gyr. Also included are the number of sources in each group with LGS stars within the error circle and the total number of LGS stars presented in each histogram. The magnitudes and colors are not corrected for reddening, due to the range of extinction values in each group of sources. However, we include a histogram of the $E(B - V)$ values, estimated as described in Section 3.2, for each set of sources in Figure 6. In Figure 7, we present histograms of the stellar colors included in each CMD. The black and red lines correspond to the same SSS grouping as in Figure 5. Most SSS are in regions of very low $E(B - V)$, but there are a larger number of sources with $E(B - V) > 0.2$ in the fields of the SSS with possible UV counterparts, indicating that in these fields there is on average a higher degree of reddening. We conclude that the UV sources overlapping with SSS have been detected in the UV not because they are in less reddened areas, but because they must be intrinsically UV brighter than the others.

We also find that the stars in the vicinity of SSS overlapping with UV sources are bluer than the population in the fields without UV detections, independently of the reddening

Table 5
Optical and UV Properties of Selected Candidate Counterparts

SSS	R.A. (J2000.0)	Decl. (J2000.0)	Mv	$B-V$	$U-B$	$(V-R)$	$R-I$	FUV	NUV	UVM2	UVW2	UVW1	$E(B-V)$	Q
XMMU-J003910.8+404521	00 39 10.84	+40 45 20.6	21.827	−0.330	−0.757	0.151	−0.17	. . .	. . .	20.35 ± 0.1	20.16 ± 0.1	20.35 ± 0.1	0.20	−0.46
RX J0039.6+4054	00 39 37.94	+40 53 07.7	. . .	. . .	. . .	. . .	. . .	. . .	. . .	20.78 ± 0.27	21.19 ± 0.28	>20.94	0.29	. . .
	00 39 39.96	+40 53 45.4	19.535	0.161	−1.052	0.159	0.147	. . .	. . .	19.02 ± 0.09	18.89 ± 0.06	18.82 ± 0.07	0.29	−1.168
RX J0040.0+4100	00 40 01.27	+41 00 51.1	22.107	−0.246	−0.859	−0.044	−0.145	19.95 ± 0.2	21.24 ± 0.2	20.89 ± 0.3	20.59 ± 0.18	>20.98	0.27	−0.682
RX J0041.5+4040	00 41 29.83	+40 40 07.0	20.813	0.081	−0.811	0.086	0.237	. . .	. . .	. . .	20.77 ± 0.25	20.60 ± 0.32	0.27	−0.869
RX J0041.8+4059	00 41 51.56	+40 59 36.2	22.224	0.135	−0.627	0.288	1.187	. . .	. . .	. . .	. . .	. . .	0.00	−0.724
	00 41 48.69	+40 59 14.9	21.688	−0.157	−0.692	0.132	0.691	. . .	. . .	. . .	. . .	. . .	0.00	−0.579
	00 41 49.62	+40 59 21.9	21.063	0.944	0.509	0.574	0.694	. . .	. . .	. . .	. . .	. . .	0.00	−0.171
RX J0042.2+4048	00 42 16.78	+40 48 14.4	19.419	−0.104	−0.993	−0.013	−0.010	17.23 ± 0.1	17.45 ± 0.04	. . .	. . .	. . .	0.30	−0.918
XMMU-J004329.8+410308	00 43 27.83	+ 41 03 08	22.786	−0.487	−1.267	−0.096	−0.316	19.26 ± 0.24	20.04 ± 0.23	. . .	. . .	. . .	0.28	−0.916
RX J0043.7+4127	00 43 45.31	+41 27 19.08	20.599	−0.090	−0.776	0.010	0.041	. . .	. . .	19.13 ± 0.12	19.23 ± 0.11	19.43 ± 0.17	0.00	−0.711
	00 43 44.71	+41 27 33.3	18.084	0.513	−0.157	0.335	0.348	. . .	. . .	19.74 ± 0.19	19.61 ± 0.14	19.17 ± 0.14	0.00	−0.526
	00 43 43.40	+41 27 15.4	20.688	0.197	−0.746	0.258	0.318	. . .	. . .	20.04 ± 0.23	19.72 ± 0.16	20.09 ± 0.28	0.00	−0.888
	00 43 44.49	+41 27 26.0	. . .	. . .	. . .	. . .	. . .	. . .	. . .	19.78 ± 0.19	19.77 ± 0.16	19.99 ± 0.27	0.00	. . .
RX J0045.4+4154	00 45 27.78	+41 54 07.7	20.286	0.028	−0.927	0.060	0.040	18.37 ± 0.35	18.70 ± 0.06	19.36 ± 0.12	19.27 ± 0.09	19.24 ± 0.10	0.52	−0.947
RX J0045.5+4206	00 45 32.74	+42 07 05.7	20.278	−0.009	−0.932	0.031	0.090	. . .	. . .	. . .	. . .	. . .	0.47	−0.926
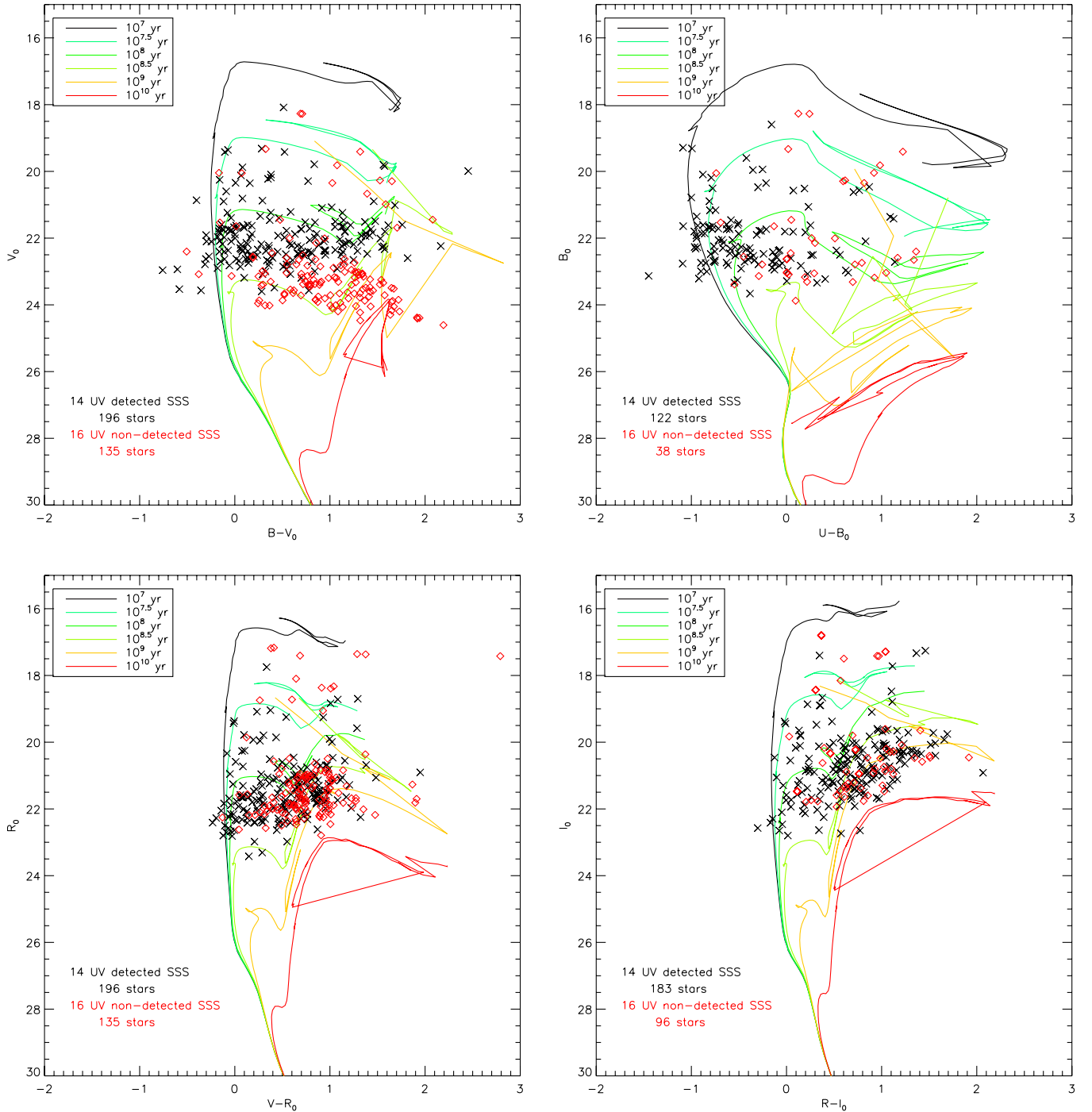
Figure 5. Optical CMDs of LGS stars within the error circles of each SSS. The magnitudes have not been corrected for reddening. The SSS are split into two groups—UV detected (black crosses) and UV non-detected (red crosses). The number of each type of source with LGS stars within the error circle, along with the total number of stars presented, is given in the lower left of each figure. Padova isochrones for $Z = 0.019$ stellar populations of ages 7–10 Gyr with $E(B-V) = 0$ are plotted in solid lines.

(A color version of this figure is available in the online journal.)

correction. The population in the SSS fields with UV counterparts also appears, particularly in the B versus $U-B$ diagram, to be on average younger. However, the ages of massive stars (most likely to be detected in UV) cannot be determined exactly by evaluating the color indices, because of degeneracy in the color space (see Massey 1998).

We used the so-called reddening-free index Q, given by

$$Q = (U - B) - 0.72(B - V) \qquad (5)$$

to select the youngest or most massive stars. Stars with spectral type earlier than B5 have Q-values close to -1, so the presence of a large number of objects with a large negative parameter near the SSS indicates that they overlap with, or are located in a young stellar population. We calculated to characterize the age of the stellar populations in the vicinity of each source. Figure 8 shows Q versus V for stars inside the SSS error circles with U bright objects detected in the *GALEX* images. Although there is some scatter, many more objects with $Q < -0.8$ are near the
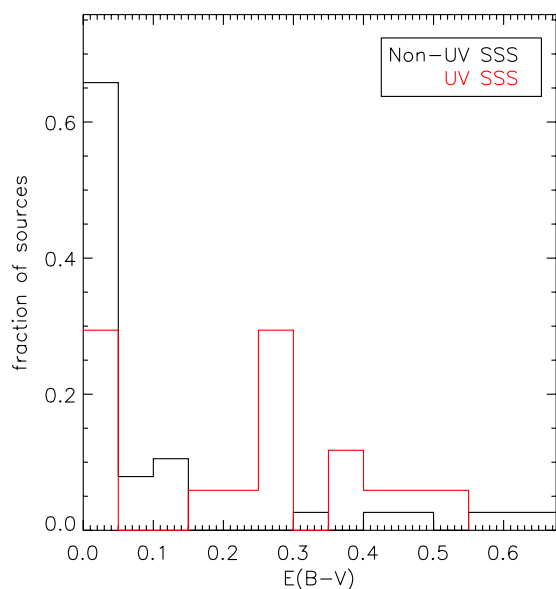
Figure 6. Histogram of $E(B-V)$ values for SSS not detected in the UV (black), and those with at least one UV source in the spatial error circle (red). The y-axis gives the fraction of SSS in each group at each reddening value.

(A color version of this figure is available in the online journal.)

SSS with possible UV counterparts. We conclude that the SSS coincident with UV objects are in younger regions of M31, and that the UV sources are young, massive stars.

The spatial coincidence of a group of SSS in other galaxies with spiral arms has been noted in other galaxies including the face on spirals M101 and M83 (De Stefano et al. 2003) and M33 (Pietsch et al. 2004a). Most important, recently three SSS of the Magellanic Clouds have been identified with high-mass X-ray binaries (hereafter HMXBs) by Kahabka et al. (2006), Takei et al. (2008), and Oliveira et al. (2010). This growing evidence suggests that also the spatial coincidence of a number of SSS in M31 with very young stars probably is physical, rather than an effect of the line of sight.

6. CLOSE UP "PORTRAITS" OF INDIVIDUAL SOURCES

In this section, we examine some of the most intriguing sources with proposed counterparts in Table 5, and an additional remarkable object in the M31 core (a total of seven SSS). From the optical and UV colors, the X-ray and optical variability, and the optical spectrum of one of the possible counterparts, we concluded that four of these sources can only be associated with O and B stars, while two are quite likely to be massive, hot hydrogen-burning WDs with an undetected companion of
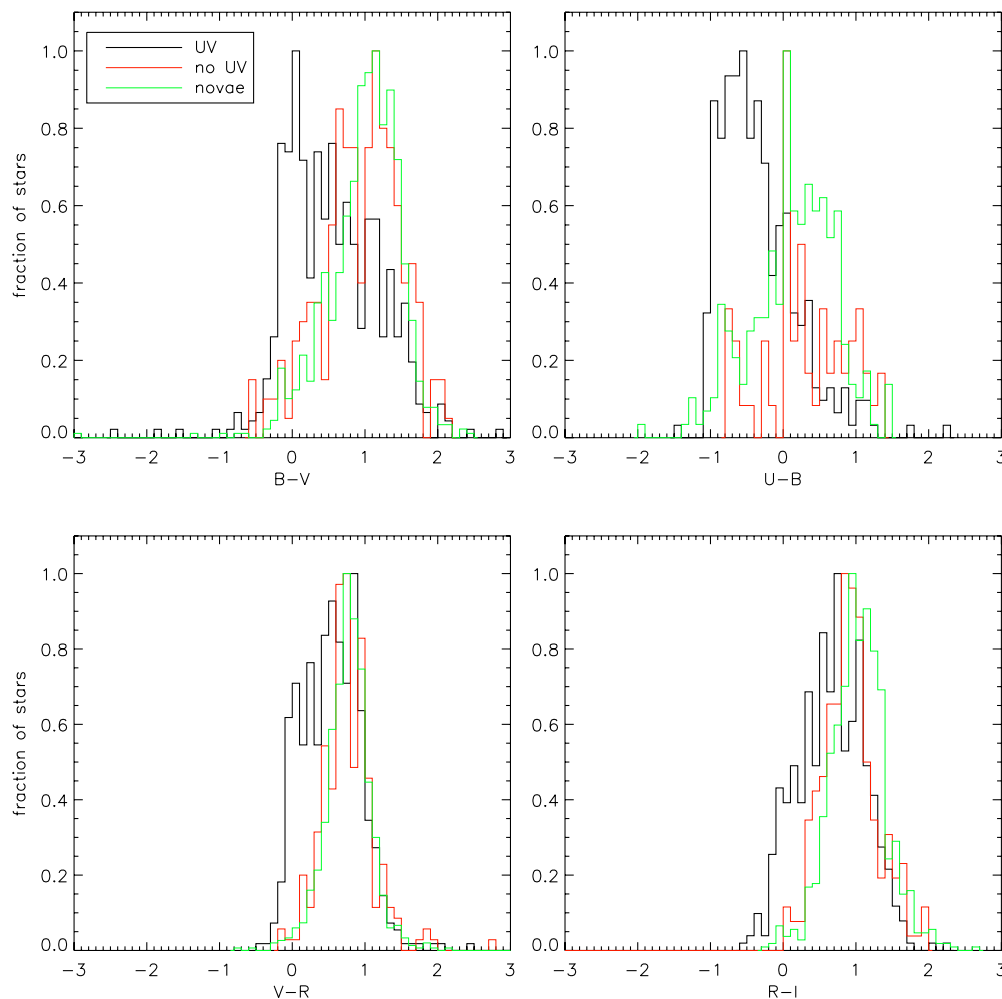
Figure 7. Normalized histograms of stellar colors of all the objects within the 2σ positional error circle of SSS with a UV detection (black) and those without (red). The population in the error circles of novae is represented in green, and follows the distribution of the non-UV detected sources (it is thus older). The $U-B$ and $R-I$ histograms contain different numbers of stars from the $B-V$ and $V-R$ histograms, because some stars were not detected in either U or I.

(A color version of this figure is available in the online journal.)
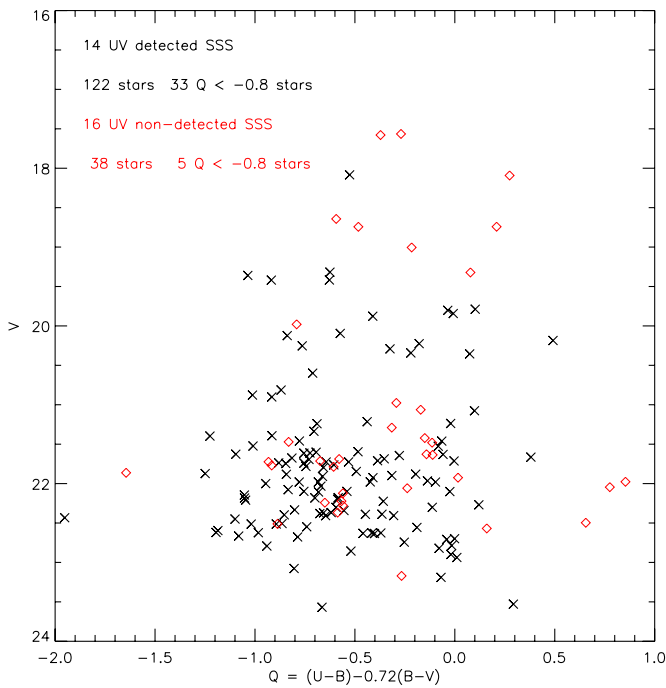
Figure 8. Reddening free Q parameter for stars within the 2σ X-ray error circles of UV detected (black) and non-detected (red) SSS. We have included the number of SSS in each group, the total number of stars associated with each group, and the number of stars with $Q < -0.8$ found for each group.

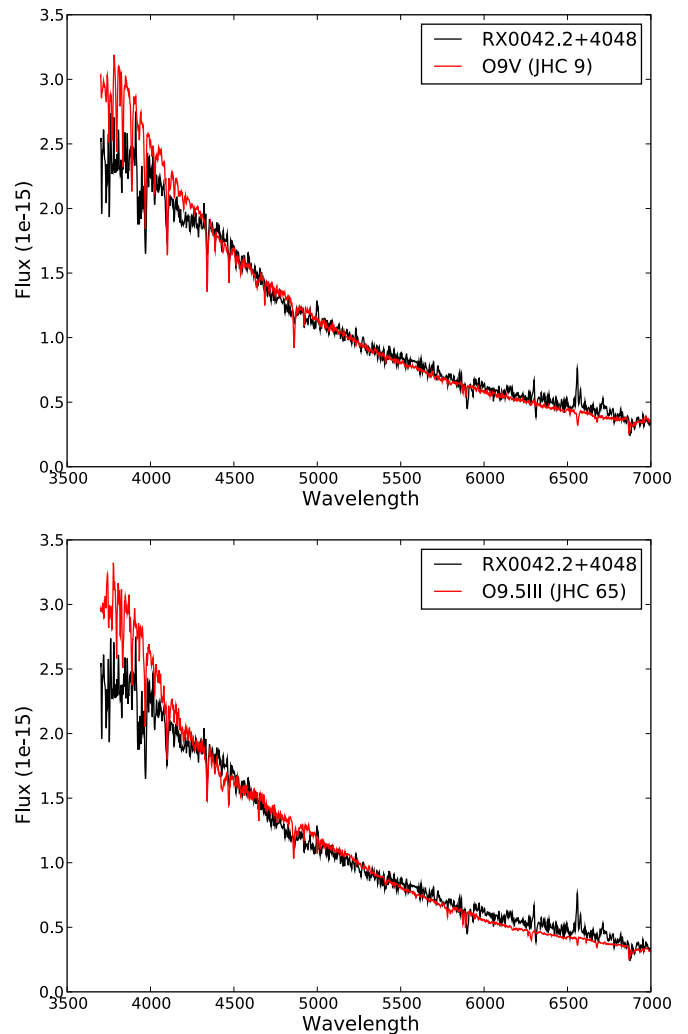(A color version of this figure is available in the online journal.)

mass below $2\,M_\odot$. The last SSS may have been an optically unobserved classical nova, but there is a massive star even in its position error circle.

6.1. RX J0042.2+4048, not an SNR

For three of the sources in Figure 4, the UV and optical color indices and the position in the H-R diagram are consistent with O or early B stars. Whatever the origin of the X-ray emission at the time of the *ROSAT* observation, it was not the present source of UV emission, which is the massive star detected also at optical wavelengths. Is the massive star in a binary, and did the measured X-ray flux originate in a compact object in this system? RX J0042.2+4048 is the only SSS associated with a star formation region that appears to be a persistent source.

We obtained an optical spectrum of the candidate counterpart of RX J0042.2+4048 with the Telescopio Nazionale Galileo (TNG) of the Italian National Institute of Astrophysics (INAF) and the DOLORES low-resolution spectrograph and camera. We used the LR-B grating and a slit width of 1 arcsec to cover the spectral range 350–800 nm with a spectral resolution of about 1.2 nm. The slit height was about 8.5 arcmin and the total exposure time was 2700 s. These data were reduced and calibrated using standard IRAF procedures. The spectrum is shown in Figure 9, dereddened using the empirical formula of Cardelli et al. (1989), implemented in the IRAF task *deredden*. We assumed $E(B-V) = 0.28$, only slightly higher than the value obtained with the method of Section 3.2 ($E(B-V) = 0.30$; see Table 5).

RX J0042.2+4048 was classified as a candidate SNR By Pietsch et al. (2005b) because they noted the overlap with the star forming region. However, the lack of S II in emission rules out the SNR interpretation. This is not surprising, because supernovae explode in cavities in regions of ongoing star formation, so they seldom leave an immediately optically


Figure 9. Optical spectrum of RX J0042.2+4148, obtained in 2009 February, and comparison with an O9.5 III and an O9 V stellar templates.

(A color version of this figure is available in the online journal.)

detectable remnant or an X-ray source. The SNRs in Table 2 are not associated with star formation regions. In Figure 9, we match the spectrum with that of HD12223 (no. 9 in Jacoby et al. 1984) classified by the authors as a O9V star and HD 16429 (no. 65 of Jacoby et al.), an O9.5III star. The first one gives the best fit, the second one is also a reasonable match. We also tried another method, the automatic algorithm implemented in the IDL code Hammer (Covey et al. 2007), that indicates a spectral type O8. The reddening free Q index in Table 5 indicates an O8 spectral type, independently of the luminosity class. The optical magnitude $V = 19.4$ (see Table 5) corresponds to an absolute visual magnitude -5, adopting a distance modulus 24.4 for M31. The absolute magnitude-spectral class given by Walborn (1972) indicates that class V O8 stars have a mean absolute magnitude of -5.0, while O8 III are at absolute magnitude -5.3, and O9 III at -5.7. We concluded that the spectrum and magnitude of RX J0042.2+4048 are typical of a late O star, perhaps a somewhat evolved one.

The star appears to be surrounded by an H II region emitting Hα (it may embed the star, or be in the background or foreground). However, with the quality of the data we are not able to rule out that some Hα emission is also due to the central object (possibly due to ongoing accretion if the O star is in a binary).
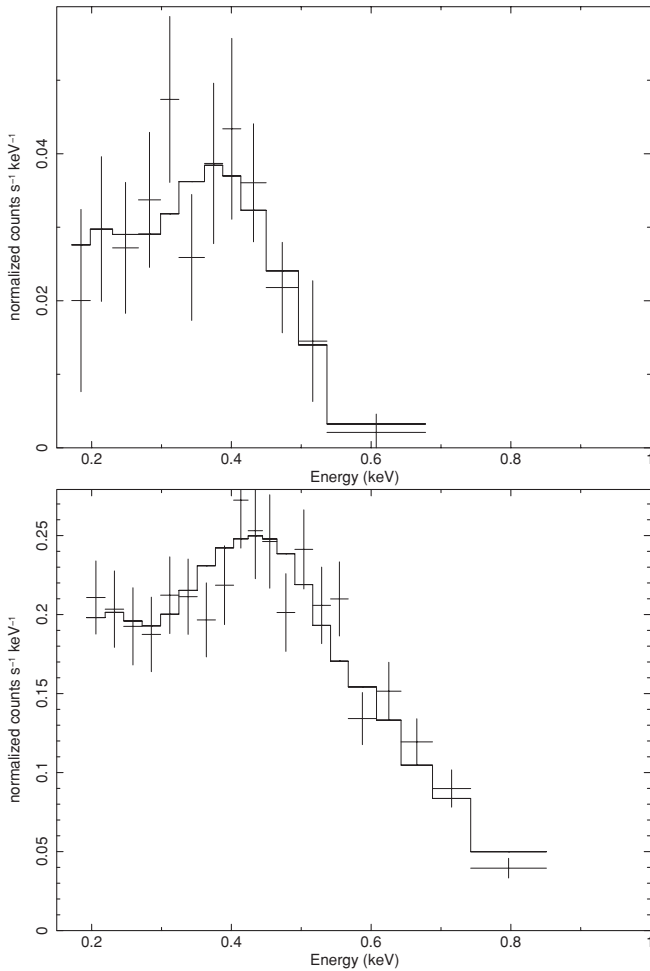
Figure 10. Upper panel: EPIC-pn spectrum of XMMU J003910.84+404520 obtained on 2006-07-23, with a best-fit blackbody model of temperature 0.05 keV, and $N(H) = 1.2 \times 10^{21}$ cm^{-2}. Lower panel: EPIC-pn spectrum of Nova 1997 12b, extracted cutting out the central region of the star's image to mitigate pile-up. The fit with an atmospheric model with depleted C is shown, with $T_{eff} = 904,000$ K, and $N(H) = 5.7 \times 10^{20}$ cm^{-2}. The X-ray luminosity in the 0.15–1.5 keV range is about 3×10^{38} erg s^{-1}.

6.2. Two New SSS in XMM-Newton Images: High-mass X-ray Binaries?

We discovered the new SSS XMMU J003910.84+404520 in *XMM-Newton* archival observation 0402560701 (PI Pietsch), as one of the brightest sources in this field, with a total EPIC-pn count rate 0.0179 ± 0.0032 counts s^{-1}. All counts are at energy below 1 keV (see Figure 10(a)). The source was not observed in either of the MOS instruments—in MOS-1 it fell on an unused CCD, and in MOS-2 in the gap between chips. The observation was disturbed by a high level of background soft proton flares, that made large portions of the exposure unsuitable for spectral analysis. The X-ray spectrum observed in the "good" time interval of about 12 ks is shown in Figure 10. Reasonable fits are obtained for blackbody models with temperatures in the range $(5–6) \times 10^5$ K and column densities $N(H)$ in the range $(0.7–1.5) \times 10^{21}$ cm^{-2}. The best fit is also shown in Figure 10a. The unabsorbed luminosity is in the energy range 0.15–8 keV of $\sim 4 \times 10^{37}$ to 10^{38} erg s^{-1} at the 2σ confidence level. As Table 5 shows, a bright NUV and FUV *GALEX* counterpart is observed the 1σ spatial error circle of the *XMM-Newton* position, which appears in the LGS as an isolated extremely blue star with $M_v = 21.827$. Magnitude and color indices are consistent

with a young, probably already evolved M31 star of spectral type B.

We requested a target of opportunity (TOO) observation of this SSS with the XRT on board the *Swift* satellite in late May of 2008, 22 months after the first detection, but XMMU J003910.84+404520 was not detected again during the 11 ks observation, with an upper limit to the X-ray luminosity $L_x < 10^{36}$ erg s^{-1}, implying that it faded by a factor >50 during the intervening months since the initial observation. No optical or UV images were taken with the OM at the time of the *XMM-Newton* detections. The timescale over which this new source faded fits both the *ROSAT* SSS and that of classical novae. However, the spatial association with the O star seems quite compelling, so we would like to suggest the intriguing possibility of a nova-like phenomenon in a massive binary. Such a "nova," or we may later define it a "pseudo-nova," would have been intrinsically much more luminous at quiescence than a classical nova with a low-mass companion. The maximum amplitude of the outburst would not exceed 5 mag, unlike 8–15 mag of amplitude of low-mass binary novae, so it may have been missed in M31.

We discovered a second short-living SSS in more recent *XMM* observations of 2008 January and February. This is XMMU J004329.8+410309, for which position and count rate are only poorly determined (we estimate a 4 arcsec uncertainty in the position and a possible $\simeq 25\%$ error in the count rates), because the source is partially imaged on a row of defective pixels in both *XMM-Newton* EPIC-pn observations. The EPIC-MOS exposures were carried out with the medium filter and the detection of this extremely soft object is very marginal, less than 3σ above the background. Notwithstanding this problem, the detection is real and the source is extremely soft, with all photons above the background below 1 keV. The count rate lower limit was 0.0092 counts s^{-1} in January and 0.0794 s^{-1} in February. This SSS was not detected in earlier observations, nor in July of 2007 and 2008, only half a year before and after the first appearance. There is only one UV counterpart, whose UV colors are shown in Figure 4, and it is the closest object to the *XMM-Newton* position in the LGS. The data, shown in Table 5, indicate an early B or a late O star. This object has a Q parameter close to -1, like RX J0042.2+4048, which we identified with an O star.

6.3. r3-8 (RX J0043.3+4120), a Source in Front of a Dust Lane?

This SSS, observed at times as one of the most luminous X-ray sources in the M31 field since the *ROSAT* survey of M31, has been described by Orio (2006). Williams et al. (2006b) suggested that it is a candidate polar CV in the foreground. This is now ruled out because there are no objects brighter than magnitude 23.5 in B and R in WIYN optical images, within 2 arcsec from the *Chandra* position (see also Orio 2006). Very deep archival *HST* deep WFPC2 images, obtained in the framework of a microlensing project, recently became available in the F841W (I) and F555W (V) filters. The images reach at least 25th magnitude and a few objects are detected within an arcsecond from the *Chandra* position. We discuss photometric measurements and possible variability of these counterparts in a forthcoming paper (M. Orio et al. 2010, in preparation). None of the possible counterparts is detected in the UV *GALEX* images (again, a magnetic CV would be detected). An isolated or binary cooling neutron star in the foreground seems also unlikely because r3-8 is very variable, even spectrally (see Figure 4 of

Orio 2006). The possibility of a background counterpart is also very unlikely because r3-8 overlaps with a dust lane in M31 (J. Gallagher, 2009, private communication); thus the detection in the easily absorbed supersoft X-rays seems to place it in front of the dust lane.

When the count rate peaks, a blackbody with a temperature in the range 60–100 eV fits only by also adding a second component because of the remaining flux in the 1–2 keV range. Altogether, the spectrum is more complex and appears different from the one of the classical novae, but we have poor statistics for a rigorous analysis. In X-rays, r3-8 remained an SSS for almost 20 years, but there are "off" states, exactly like in the LMC source CAL 83. In some observations the SSS falls in fact below the detection threshold (see Table 2). With *XMM-Newton* it was observed to gradually decrease in luminosity in four closely spaced observations of 2007 December–2008 February (see Table 1, note that the source is on a CCD junction on one of the five exposures). The average count rate varied from 0.0336 ± 0.0023 counts s^{-1} to 0.0017 ± 0.0001 counts s^{-1} in the 0.15–1 keV range, but we could not detect any short-term variability on timescales of minutes like for r2-12 (see the next section). When the source was re-observed in 2008 more than five months later in July, the count rate had jumped again to a level above 0.0450 ± 0.0033 counts s^{-1} (this was again only a partial observation because the source was partially hidden by a CCD junction). It is unfortunate that this SSS often fell in the gap between chips. In the future, more detailed, dedicated temporal coverage should allow us to obtain the exact timescales (duration of low and high states) that are essential to understand the nature of this intriguing object.

6.4. r2-12, the Ongoing Firework

This SSS is not included in our search for UV and optical counterparts because it is in the central region of M31. However, B. Patel et al. (2010, in preparation) show that its only possible counterparts in *HST* images are red stars of magnitude ⩾24, ruling out a foreground object. In four *XMM-Newton* exposures taken between 2000 and 2004 Trudolyubov & Priedhorsky (2008) measured a period of 217.7 s, which they interpret this as the spin period of a massive WD burning H in a shell in a close binary. As we show in Figure 11, the period was still detected in 2008 (the light curve of 2008 July, folded with this period is shown in Figure 11, upper panel). We do find this periodicity in most, but not in all the uninterrupted observations done in recent years. In some observations, especially in early 2008, also several other periods ranging from few minutes to 2 hr are measured, like in Nova V4743 Sgr (Leibowitz et al. 2006). Detailed temporal analysis will be in a dedicated paper.

r2-12 is the second SSS in M31 with coherent X-ray flux pulsations, after the transient supersoft source XMMU J004319.4+411758 with an 865.5 s pulsation period (Osborne et al. 2001). The *XMM-Newton* data of r2-12 are affected by heavy pile-up and the PSF overlap with the PSF of other sources. There is one long *Chandra* ACIS-S observation, but this instrument is not sensitive to the softest portion of the spectrum. We did attempt a preliminary fit with atmospheric models and find a WD atmospheric temperature around 900,000 K (with the atmospheric model studied for V4743 Sgr, Rauch et al. 2010, applied also to RS Oph, see Nelson et al. 2008), with estimated error bars of about ±100,000 K. A second "disk blackbody" low-luminosity component improves the fit, as shown in Orio (2006). If r2-12 is an accreting and hydrogen-burning WD, it is extremely hot and it has remained at a high-luminosity level
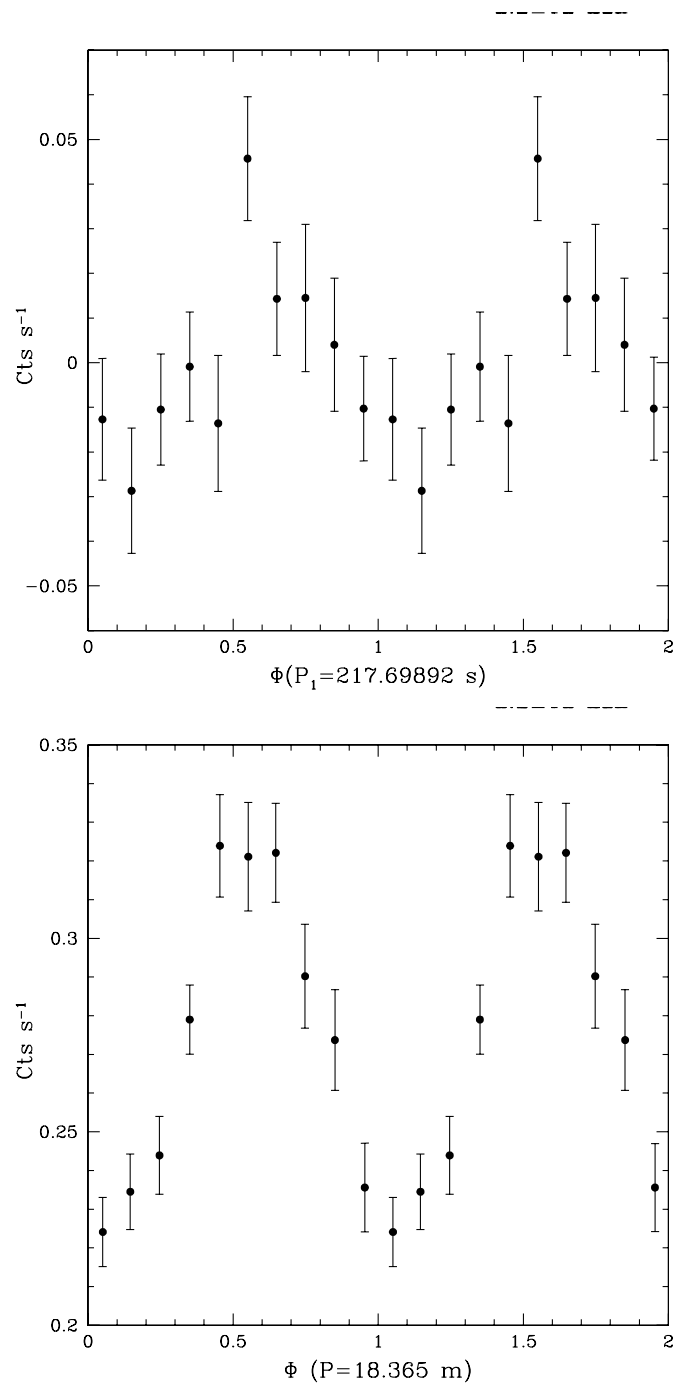
Figure 11. Upper panel: light curve of source r2-12, binned every 50 s and folded with the 217 s period for the *XMM-Newton* observation of 2008 July (above); lower panel: light curve of Nova M31 2007-12b observed with *XMM-Newton* in 2008 February and folded with the 18.365 minute period.

since the first observation in 2000. The X-ray luminosity at the distance of M31 reaches 10^{-39} erg s^{-1} in some observations, although there are remaining uncertainties because the estimated unabsorbed flux is model dependent.

If r2-12 is indeed in M31, the only comparable Local Group SSS for high bolometric luminosity and long-term life as an SSS is CAL 83 in the LMC (Greiner et al. 2008), although CAL 83 experiences periodic "X-ray off" states (Greiner & Di Stefano 2002; Lanz et al. 2005). However, CAL 83 is at least 1 mag optically more luminous than any candidate optical counterpart of r2-12.

Table 6
WIYN Observations of *ROSAT* SSS in M31

Source	Date of Observation	Filter	Exp Time (s)
RX J0041.8+4059	2004 Sep 16	B	5 × 1200
	2004 Sep 16	V	2 × 600
	2004 Sep 17	B	6 × 1200
	2004 Sep 29	B	15 × 1200
	2004 Oct 7	B	4 × 1200
	2004 Oct 9	B	5 × 1200
	2004 Oct 11	R	3 × 120
	2004 Oct 11	B	5 × 1200
	2005 Oct 23	B	20 × 900
	2005 Oct 24	B	23 × 900
	2005 Oct 24	R	3 120
	2006 Sep 29	B	8 × 1200
RX J0045.5+4206	2004 Oct 7	B	2 × 1200
	2004 Oct 9	B	5 × 900
	2004 Oct 9	R	180
	2004 Oct 10	B	4 × 900
	2004 Oct 10	Hα	1200
	2004 Oct 10	R	180
	2004 Oct 11	B	5 × 1200
	2004 Oct 11	R	180
	2004 Oct 11	Hα	1200
	2005 Aug 27	B	10 × 1200
	2006 Sep 29	B	2 × 1200
	2006 Sep 29	R	120
r3-8	2005 Jun 16	B	2 × 900
	2005 Jun 16	R	420
	2005 Jun 17	R	3 × 60

6.5. Long-term Monitoring of RX J0041.8+4059 and RX J0045.5+4206 with WIYN

The fields of two *ROSAT* SSS—RX J0041.8+4059 and RX J0045.5+4206—were monitored by us with the WIYN 3.5 m telescope. A list of the WIYN exposures is in Table 6. The limiting magnitude of the images varied from night to night between 23rd and slightly fainter than 24th magnitude. We searched for orbital variability, known to exist in several Magellanic Clouds SSS (e.g., Orio et al. 1994, 1997). The fields of the two sources we chose have at least one unusually blue star within the 2σ X-ray positional error circle (see Table 5). RX J0041.8+4059 was only detected in the first PSPC survey, but with a higher count rate than most other *ROSAT* SSS. It may have been a nova because of its high flux and quick disappearance. RX J0045.5+4206 was detected in at least three occasions over two years (see Greiner et al. 2004) and it is close to the A107 OB association (van den Bergh 1964). A large nebula detected within the error circle of RX J0045.5+4206 in the *U*-band images was initially thought to be associated with the SSS, but is instead associated with of a nearby Wolf–Rayet star (Greiner et al. 1999).

WIYN observations of RX J0041.8+4059 were carried out on seven nights in 2004 September and October, 2005 October, and 2006 September (see Table 6). RX J0045.5+4206 was observed on four nights in 2004 October and 2005 August. Since we immediately identified a marginally short-term variable object in the field of RX J0041.8+4059, we continued the short-term monitoring for this source. RX J0045.5+4206 is in a region of young massive stars, so we were particularly interested in variability exists on longer timescales of months or years, expected for a HMXB. We rule out photometric variability by more than 0.002 mag in any of the possible counterparts in the *ROSAT* error circle of RX J0045.5+4206, timescales of

hours to months. There is a marginally variable object in the error circle of RX J0041.8+4059 but it is not a very blue star (the third candidate in Table 5). The high visual magnitude, $V = 18.084$, rules out that this variable object is a classical nova at quiescence. Optical spectra of the first candidate in Table 5 indicate instead a young and massive star (J. Greiner & R. Schwarz 2008, private communication).

In conclusion, both objects have possible massive stars as counterparts, although RX J0041.8+4059 is not in a star formation region and thus we cannot rule out a classical nova, now beyond detection threshold at quiescence. For RX J0045.5+4206, the association with a massive star is more compelling, so this SSS is more likely to be a massive binary, although we could not detect an orbital period.

7. CLASSICAL AND RECURRENT NOVAE AS SSS

As we discussed above, approximately 30% of all SSS discovered in M31 are classical novae (see Table 3). Given the transient nature of many of the non-classified SSS in the M31 population, it is not unlikely that a fraction of these sources are also novae whose optical outbursts were missed. At the time of the *ROSAT* surveys of M31, optical monitoring for transients in M31 was not very comprehensive, and nova outbursts (especially those of fast novae) may have been frequently missed. In the last few years, a number of M31 monitoring programs aimed at detecting transient novae have been started.[8] With more thorough monitoring, it is likely that almost all recent nova outbursts have been observed if they did not occur during the seasonal observing gap. We cross correlated the 794 classical novae in outburst between 1912 and 2008 with all the SSS in M31. Even the oldest novae were included, because they may be recurrent novae and have had new, more recent outbursts. Four hundred and sixty-three novae were outside the central area and can be resolved in the UV images and with *XMM-Newton* in X-rays. Although there are some notable novae with very short SSS duration, the timescales of the SSS phase of novae in M31 are on average longer than in the Galaxy (as detected with *Swift* and other instruments; M. Orio 2010, in preparation). This is consistent with the nova theory, assuming that envelope material is left over in novae that accrete more mass before the outburst. A larger envelope is in fact accreted by novae on low-mass WDs, which need more time to build the required pressure for the thermonuclear flash. In the core of M31 there is little interstellar gas, so it is "transparent" to novae (unlike our Galactic bulge). This region hosts a large, predominant old population with lower mass WDs, and is a window for detection of many low WD mass novae.

Some of the brightest and longer-lasting transient X-ray sources detected exactly at the optical positions and around the outburst time of novae with *Chandra* HRC-I (not included in Table 3) have been identified with Novae M31 1997-11a, 1999-10a, 2004-09b, 2004-11f, 2007-06b, and 2007-11a. Nova M31 1997-11a had a very fast decline in both optical and X-rays and has been ascribed to a very massive WD (Henze et al. 2009). It is also interesting to mention that with the HRC-I, some X-ray sources are also discovered at the positions of some old novae, Novae M31 1920-09a, 1923-12b, 1954-08a, and 1960-09a. If the spatial coincidence is not a mere random coincidence, these are more likely to be recurrent novae rather than classical novae undergoing extremely long SSS phases.

---

[8] A list of all novae announced in M31 is maintained by W. Pietsch, and is publicly available at http://www.mpe.mpg.de/~m31novae/.

Table 7
Classical Novae Detected in *GALEX* Images

Nova ID	R.A. (J2000.0)	Decl. (J2000.0)	$E(B-V)$	t_0 (JD)	Obs_{UV} - t_0 (days)	m_{FUV}	m_{NUV}	$E(B-V)$
M31N 2003-06b	00 43 36.17	+41 16 39.4	0.08	2452815.51	72.84	18.24 ± 0.09	18.86 ± 0.07	0.17
⋯	⋯	⋯	⋯	⋯	106.27	18.92 ± 0.12	20.31 ± 0.25	
M31N 2003-07a	00 42 02.93	+41 05 01.5	0.00	2452847.48	40.87	19.10 ± 0.16	18.73 ± 0.16	0.09
M31N 2003-09a	00 42 59.84	+41 03 33.9	0.25	2452899.66	−11.31	18.34 ± 0.13	18.74 ± 0.10	0.34
⋯	⋯	⋯	⋯	⋯	22.12	17.98 ± 0.08	18.51 ± 0.07	
M31N 2006-10b	00 39 27.38	+40 51 09.8	0.16	2454039.59	6.78	18.15 ± 0.22	17.75 ± 0.08	0.25
M31N 2007-07f	00 38 42.20	+40 52 56.0	0.00	2454292.48	66.2	19.10 ± 0.10	19.67 ± 0.13	0.09
⋯	⋯	⋯	⋯	⋯	66.4	18.94 ± 0.10	19.64 ± 0.10	
M31N 2007-08d	00 39 30.27	+40 29 14.2	0.25	2454336.58	22.1	19.15 ± 0.16	18.31 ± 0.05	0.34
⋯	⋯	⋯	⋯	⋯	22.3	18.44 ± 0.16	18.44 ± 0.05	

Note. Luminosities and colors are based on the de-reddened magnitudes obtained using the quoted extinction.

We would like to focus on one SSS among all the M31 novae in recent years, because it bears strong similarities to the recurrent nova RS Oph, believed to be an SN Ia progenitor (see Nelson et al. 2008 and references therein). This is Nova 2007-12b, which had an extremely fast X-ray evolution. It was detected in X-rays with *Swift* after only 34 days after the first observation around maximum days, and after six months the X-ray source was no longer detected with *XMM-Newton*. The high effective temperature and luminosity resemble RS Oph (Nelson et al. 2008), and so does the short timescale of the evolution. As Figure 8 shows, a clear periodicity of 1101.93 s is detected in the power spectrum (see lower panel of Figure 11). The amplitude of the modulation is a little above 5%. This period is likely to be the spin period of the WD, like for the Galactic nova V4743 Sgr, another luminous SSS (Leibowitz et al. 2006). The X-ray luminosity was above 10^{38} erg s^{-1} after two months, with a WD atmospheric temperature 760,000 K (lower panel of Figure 10). This M31 nova appears to have been a truly exceptional object like RS Oph, probably with a WD mass very close to the Chandrasekhar value.

Of the 463 novae included in our UV search, only seven are detected as UV transients in the *GALEX* images (Table 7), about 10% of the total number of novae observed in outburst in the year before the two *GALEX* observations. No nova has been detected in UV more than 107 days after the observed optical maximum. The vega magnitudes in the NUV and FUV *GALEX* bands, as well as other properties, are given in Table 7. The luminosities are in the range 5.3×10^{36}–1.9×10^{38} erg s^{-1} after correcting for reddening. We note that where a nova is detected in multiple survey pointings after outburst, we observe a blueward color evolution as is expected as the nova photosphere recedes because of mass loss. For the majority of the detected novae, the *GALEX* colors indicate that they were observed while the envelope was still rather extended and cool. Only in the second observation of Nova 2003-06b, carried out 106 days after the outburst, the *GALEX* color index is -0.74 ± 0.27—consistent with emission from a hot, compact object. The distribution of the novae is plotted in green in Figure 7. The figure demonstrates that the host stellar population of novae is much more similar to that of the SSS with no UV counterparts than the UV detected SSS. We performed the Student's *t*-test, to compare the means of two distributions. The host populations of the novae and the UV non-detected SSS have the same mean value of $(B-V)$ at the 95% confidence level. Comparing $V-R$, the confidence level is 76%, although we note that the measured mean values of the two distributions differ by only 0.03 mag. Thus, the non-UV-bright SSS lie in the same population as classical novae,

generally not a very young population. A similar test to compare the UV luminous sources (associated with young stars) to the classical nova population rejects the null hypothesis at the 98% level, showing that these sources reside in significantly different populations.

The type of population, the transient X-ray behavior, and the lack of UV detections seem to indicate that the unidentified, transient SSS in M31 that do not reside in areas of star formation were probably classical novae, whose optical outbursts were missed. For instance for XMMU J004319.4+411758, source 38 in Table 2, the supersoft X-ray flux was pulsed with an 865 s period (Osborne et al. 2001; King et al. 2002), which is very similar to the oscillations discovered in the X-ray flux of some Galactic novae (e.g., Drake et al. 2003; Leibowitz et al. 2006) and in Nova 1997 12b.

8. SSS AS YOUNG, MASSIVE BINARIES

We have shown that 20% of the M31 SSS, representing about 35% of the unidentified sources, are in regions of young stellar populations (yellow and orange portions of the histogram in Figure 1). Are these binaries, and do they host accreting and H-burning WDs like their low-mass counterparts? WDs in HMXB are likely to exist, because stars of mass up to $\sim 10\,M_\odot$ end their lives as WDs. O and B stars with massive WD companions have been observed (e.g., y Pup, Vennes 2000; θ Hya, Burleigh & Barstow 1999; and 16 Dra, Burleigh & Barstow 2000). These WDs are more massive than $0.8\,M_\odot$, since their progenitors must have been of an earlier spectral type than the companion, which is itself an early-type star. The systems observed so far are in rather wide binaries (periods of days rather than hours as observed in CV systems), and therefore mass transfer onto the WD via Roche lobe overflow is unlikely. O and B stars lose mass at rates up to $10^{-7}\,M_\odot$ yr^{-1} in winds, but the efficiency of wind accretion onto the WD is low.

However, a special evolutionary path for WD binaries in young populations, involving Be stars, has been discussed in the literature. Be stars are B stars of spectral class V–III that exhibit emission lines in their spectra, thought to arise in a circumstellar disk extending up to a few hundreds $R_\odot$ from the star (Tavani & Arons 1997). They rotate rapidly, at rates between 70% and 100% of the critical rotation velocity (Townsend et al. 2004), and it is this rapid rotation that seems to be responsible for the formation of the disk. About 40 Be stars in the SMC have neutron star companions (Galache et al. 2008) and McSwain & Gies (2005) in a recent photometric survey of open clusters found that up to 73% of Be stars may have been spun up by binary

evolution. In systems with a less massive primary than $10\,M_\odot$, the degenerate companion must be a WD, and such binaries significantly outnumber the Be/neutron star X-ray systems due to the larger number of WDs produced in any stellar population.

The formation of massive WD binaries has been explored in detail by several authors, including Waters et al. (1989), Pols et al. (1991), and Raguzova (2001). Raguzova predicts that some 40% of Be stars formed by binary evolution eventually have a CO WD companion, mostly of mass in the range $0.8–1\,M_\odot$ (before accreting mass from the companion, if this happens). This evolutionary path is particularly interesting to us because CO WDs are the ones that may end as SNe Ia. WD companions of much higher mass, above $1.2\,M_\odot$, originate from stars with ONe cores, and are likely to end their evolution instead with an accretion-induced collapse producing a neutron star. Raguzova's (2001) results thus imply that many SSS in HMXB may end as SNe Ia. The orbital periods for CO WD close binaries in this model are $\sim$50–300 days and the component separations of less than a few hundred $R_\odot$, placing the WD orbit inside the disk of the Be star. Since the formation of a WD does not result in any angular momentum kick, the orbit is circular (unlike the eccentric orbits of Be/NS binaries) and the equatorial plane of the Be star is aligned with the orbital plane. This configuration allows accretion onto the WD, opening up the possibility of shell nuclear burning just as in classical novae. Would the mass accretion rate lead to thermonuclear flashes? Perhaps the SSS we have observed in young stellar populations in M31 are thermonuclear events in Be–WD binary systems.

The SSS studied in Section 6 probably fit this scenario. However, one other *ROSAT* source, RX J0045.4+4219 (White et al. 1995), had a new X-ray flare after only a year, a short timescale for repetition of a thermonuclear flash. Since this is the only SSS of this group that was observed to recur, the jury is still out. Even if this is still speculative, we can certainly say that at the M31 distance all of the SSS in star-forming regions have a luminosity and a temperature that are compatible with accreting and hydrogen-burning WDs. We suggest that these systems are candidate progenitors of the prompt component of SNe Ia. The evolutionary timescales are short, because Be/WD binaries form within a few 10^7 years after a starburst (Raguzova 2001). With accretion rates of order of $10^{-8}\,M_\odot\,\mathrm{yr}^{-1}$, these WDs could reach the Chandrasekhar limit in $<10^8$ years, thereby explaining the SFR-dependent component of SNe Ia (Greggio et al. 2008).

An obstacle for this scenario is the excessive amount of hydrogen, which should be detectable in the optical spectra. The absence of hydrogen may be explained with an additional mechanism that removes mass from the system. A close binary with a massive WD and a hot dwarf secondary—a sort of extreme Wolf–Rayet that has lost all its hydrogen envelope—has recently been discovered by Mereghetti et al. (2009). HMXB-SSS may have only sporadic episodes of mass transfer and hydrogen burning, culminating in a configuration where the secondary has lost its hydrogen-rich envelope like the one in Mereghetti et al.'s paper. The very rapid mass transfer occurring in that binary, as the authors underline, is bound to trigger CNO burning and the system is likely to end as an SN Ia. We suggest that the massive SSS in M31 are at a prior stage of the system studied by Mereghetti et al.

Another issue to investigate is whether the WD orbit in Be/WD binaries embedded in the disk of the Be allows detection of EUV and soft X-ray photons from the WD. Would the density in these disks not be so high to absorb the SSS flux? There is evidence that Be stars may periodically eject their disks: this phenomenon would allow sporadic detection of the shell burning WD. Time-resolved optical spectra of these SSS with large telescopes are required to better understand their nature and evolution.

9. CONCLUSIONS

Our study indicates that only about 20% of the non-classified SSS in M31 (11 out of 51 SSS that were observed again several times) did not completely turn off in X-rays and UV. For many of these objects, repeated observations seem to rule out that the cause of the turn-off is fluctuations in effective temperature drifting into the EUV range. In addition, more than half of all unidentified SSS in M31 have no UV bright counterpart at all, so they are unlikely to still be hot objects. Even if possible UV counterparts have been detected, the majority of the SSS are not as UV luminous as expected for a WD on which H-burning is still continuing. Moreover, the timescales for the X-ray decay of many luminous SSS are often those expected for classical and recurrent novae, so the post-outburst novae among SSS may represent more than half of the total population.

For comparison, among less than 20 SSS observed in the Galaxy, most were novae, two are symbiotics, and only two are persistent sources—MR Vel and Q And (e.g., see Greiner 2000; Šimon 2003). Thus the Galactic SSS statistics appear quite similar to Andromeda. The LMC data are different, because in that galaxy only two out of eight well-observed SSS were observed as novae. However, the other SSS, of which all but one are very unlikely to have been novae, are also variable or transient. In contrast in the SMC, out of seven non-nova SSS that have been monitored, only one source has become completely unobservable in many years of X-ray monitoring. Since the effective temperatures and luminosities are on average much lower in the SMC than in the LMC, we can confidently say that fluctuations in effective temperature are not the cause for the disappearing LMC sources, because they are on average much hotter than the SMC ones. The difference may be due to a selection effect, because the SMC has a smaller population but a larger volume in this galaxy is gas poor, with negligible intrinsic absorption and suitable for detection of low-luminosity SSS. The very different duty cycle may be due instead to metallicity, a possibility that should be investigated.

r2-12 and r3-8 are two SSS whose X-ray spectra are typical of extremely hot WD binaries, but the *HST* observations indicate that the absolute optical luminosities of the possible optical counterparts are at least 1 mag lower than in two massive WD systems of the LMC, CAL 83, and RX J0513.9−6951 (see Greiner 2000 and references therein). An optical counterpart with $V \leqslant 0$ is observed in two of the MC SSS WD binaries that host a low-mass secondary, namely RX J0537.7−7034 in the LMC (Greiner et al. 2004) and SMC 13 (Orio et al. 1994; Schmidtke & Cowley 1996). On the other hand, the putative WD of r2-12 and r3-8 must be massive, because the fast 217 s period of r2-12 is likely to be the spin period of a very massive WD (above $1.2\,M_\odot$) and WD atmospheric temperature is above 60 eV (expected for WDs above $1\,M_\odot$; see e.g., Rauch et al. 2010). These long-duty cycle SSS must be rare in M31, since we found only two of them, both exhibiting high effective temperature and no massive star as optical counterpart. We conclude that in M31 the single degenerate progenitors of SNe Ia are to be sought mainly among recurrent novae and symbiotic systems—objects that have only sporadic phases as SSS.

The possible optical counterparts of RX J0040.0+4100 and RX J0042.2+4048 are instead clearly massive stars, similar to three MC SSS. The UV flux of the RX J0040.0+4100 optical counterpart is higher than any O or B star, but in RX J0042.2+4048 the putative WD companion, if it exists, has already cooled. These two interesting objects, and a few other SSS in M31 that have never turned off in X-rays, should be studied more in detail, to prove the proposed classification as HMXBs. Remarkably, only 17 SSS have at least one UV counterpart in the X-ray error circle, and these counterparts are almost always massive stars. We suggest that possibly as many as a third of the observed SSS in M31 are HMXBs. The X-ray emission of SSS is several orders of magnitude more luminous than that normally associated with O/B stars, which is difficult to understand unless there is a WD and it was burning hydrogen at the time of the SSS emission.

One of these SSS, XMMU J003910.84+404520, was transient in soft X-rays on a timescale consistent with a nova. Several other *ROSAT* SSS were transient within months, like novae. A "pseudo-nova" in a massive system would only have an optical amplitude of about 5 mag above the quiescent magnitude and is more likely to be undetected. We speculate that novae in massive binaries may have been classified among luminous blue variables. Several pieces of observational and theoretical evidence indicate that a large number of WD/O-B and even more WD/Be star binaries form within the first 10^8 years after an episode of star formation. In such systems, the WDs must be significantly more massive than their counterparts in older populations. Under certain conditions, the WDs in these systems would undergo cycles of accretion and nuclear burning, as we see in CVs in older populations. Perhaps the transient SSS discovered in young populations are episodes of nuclear shell flashes without mass loss, rather than envelope ejections in nova outburst. If the WD is composed of CO and envelope growth continues, these systems may end their evolution as SNe Ia. We suggest the intriguing possibility that these are the progenitors of the component of the SNe Ia rate that is associated with young stellar populations. In the MC, where the optical identification is much more feasible, 3 out of 15 SSS observed in recent years have been identified as likely HMXBs. Future observations may prove that the SSS associated with young stars are a new class of massive close binaries with important implications for the origin of SNe Ia.

REFERENCES

Arnett, W. D. 1979, ApJL, 230, L37
Balman, S., Krautter, J., & Ögelman, H. 1998, ApJ, 499, 395
Bianchi, L., Madore, B., Thilker, D., Gil de Paz, A., & GALEX Science Team 2003, BAAS, 35, 1354
Branch, D. 1998, ARA&A, 36, 17
Burleigh, M. R., & Barstow, M. A. 1999, A&A, 341, 795
Burleigh, M. R., & Barstow, M. A. 2000, A&A, 359, 977
Cardelli, J. A., Clayton, G. C., & Mathis, J. S. 1989, in IAU Symp. 135, Interstellar Dust, ed. L. J. Allamandola & A. G. G. M. Tielens (Dordrecht: Kluwer), 5
Covey, K. R., et al. 2007, AJ, 134, 2398

Di Stefano, R., & Kong, A. K. H. 2003, ApJ, 592, 884
Di Stefano, R., & Kong, A. K. H. 2004, ApJ, 609, 710
Di Stefano, R., Kong, A. K. H., VanDalfsen, M. L., Harris, W. E., Murray, S. S., & Delain, K. M. 2003, ApJ, 599, 1067
Di Stefano, R., et al. 2004, ApJ, 610, 247
Drake, J. J., et al. 2003, ApJ, 584, 448
Fujimoto, M. Y. 1982, ApJ, 257, 767
Galache, J. L., Corbet, R. H. D., Coe, M. J., Laycock, S., Schurch, M. P. E., Markwardt, C., Marshall, F. E., & Lochner, J. 2008, ApJS, 177, 189
Garcia, M. R., et al. 2002, ATel, 82
Gilfanov, M., & Bogdan, A. 2010, Nature, 463, 924
Girardi, L., Bertelli, G., Bressan, A., Chiosi, C., Groenewegen, M. A. T., Marigo, P., Salasnich, B., & Weiss, A. 2002, A&A, 391, 195
Greggio, L., Renzini, A., & Daddi, E. 2008, MNRAS, 388, 829
Greiner, J. 1996, in Supersoft X-Ray Sources, Lecture Notes in Physics, Vol. 472, ed. J. Greiner (Springer: Berlin), 299
Greiner, J. 2000, New Astron., 5, 137
Greiner, J., & Di Stefano, R. 2002, A&A, 387, 944
Greiner, J., Di Stefano, R., Kong, A., & Primini, F. 2004, ApJ, 610, 261
Greiner, J., Schwarz, R., Sala, G., Ness, J. U., & Mennickent, R. 2008, ATel, 1357
Greiner, J., Tovmassian, G., Komossa, S., Rosado, M., & Arrieta, A. 1999, A&A, 347, 556
Haberl, F., Filipovix, M., & Pietsch, W. 2000, A&A, 142, 41
Hachisu, I., & Kato, M. 2000, ApJ, 563, L93
Hamuy, M., Phillips, M. M., Maza, J., Suntzeff, N. B., Schommer, R. A., & Aviles, R. 1995, AJ, 109, 1
Heise, J., van Teeseling, A., & Kahabka, P. 1994, A&A, 288, L45
Henze, M., et al. 2009, A&A, 498, K13
Hillebrandt, W., & Niemeyer, J. C. 2000, ARA&A, 38, 191
Jacoby, G. H., Hunter, D. A., & Christian, C. A. 1984, ApJS, 56, 257
Kaaret, P. 2002, ApJ, 578, 114
Kahabka, P. 1999, A&A, 344, 459
Kahabka, P., Haberl, F., Payne, J. L., & Filipović, M. D. 2006, A&A, 458, 285
King, A. R., Osborne, J. P., & Shenker, K. 2002, MNRAS, 329, L43
Lanz, T., et al. 2005, ApJ, 619, L517
Leibowitz, E., et al. 2006, MNRAS, 371, 424
Long, K. S., Helfand, D. J., & Grabelsky, D. A. 1981, ApJ, 248, 925
Mannucci, F., Della Valle, M., Panagia, N., Cappellaro, E., Cresci, G., Maiolino, R., Petrosian, A., & Turatto, M. 2005, A&A, 433, 807
Martin, C., et al. 2003, Proc. SPIE, 4854, 336
Mason, B. D., Hartkopf, W., & Corbin, T. 2005, BAAS, 37, 1548
Massey, P. 1998, in Stellar Astrophysics for the Local Group: VIII Canary Islands Winter School of Astrophysics, ed. A. Aparicio, A. Herrero, & F. Sanchez (Cambridge: Cambridge Univ. Press), 95
Massey, P., Olsen, K. A. G., Hodge, P. W., Strong, S. B., Jacoby, G. H., Schlingman, W., & Smith, R. C. 2006, AJ, 131, 2478
McSwain, M. V., & Gies, D. R. 2005, ApJS, 161, 118
Mereghetti, S., et al. 2009, Science, 325, 1222
Nedialkov, P., et al. 2002, A&A, 389, 439
Nelson, T., Orio, M., Cassinelli, J. P., Still, M., Leibowitz, E., & Mucciarelli, P. 2008, ApJ, 673, 1067
Nomoto, K., & Iben, I., Jr. 1985, ApJ, 297, 531
Nomoto, K., Saio, H., Kato, M., & Hachisu, I. 2007, ApJ, 663, 1269
Oliveira, A. S., et al. 2010, ApJ, submitted
Orio, M. 2006, ApJ, 643, 844
Orio, M., Covington, J., & Ögelman, H. 2001, A&A, 373, 542
Orio, M., della Valle, M., Massone, G., & Ogelman, H. 1994, A&A, 289, L11
Orio, M., della Valle, M., Massone, G., & Ogelman, H. 1997, A&A, 325, L1
Orio, M., Hartmann, W., Still, M., & Greiner, J. 2003, ApJ, 594, 435
Orio, M., Mason, E., Gallagher, J., & Abbott, T. 2009, ATel, 1930
Orio, M., Zezas, A., Munari, U., Siviero, A., & Tepedelenlioglu, E. 2007, ApJ, 661, 1105
Osborne, J. P., et al. 2001, A&A, 378, 800
Paczyński, B. 1971, Acta Astron., 21, 417
Parthasarathy, M., Branch, D., Jeffery, D. J., & Baron, E. 2007, New Astron. Rev., 51, 524
Patel, B., et al. 2008, AAS Meeting, 211, 162.28
Pietsch, W., Fliri, J., Freyberg, M. J., Greiner, J., Haberl, F., Riffeser, A., & Sala, G. 2005a, A&A, 442, 879
Pietsch, W., Freyberg, M., & Haberl, F. 2005b, A&A, 434, 483
Pietsch, W., Misanovic, Z., Haberl, F., Hatzidimitriou, D., Ehle, M., & Trinchieri, G. 2004, A&A, 426, 11
Pietsch, W., et al. 2007, A&A, 465, 375
Pols, O. R., Cote, J., Waters, L. B. F. M., & Heise, J. 1991, A&A, 241, 419
Raguzova, N. V. 2001, A&A, 367, 848

Rauch, T., Orio, M., Gonzalez-Riestra, R., Nelson, T., Still, M., & Willms, J. 2010, ApJ, 717, 363

Reinsch, K., van Teeseling, A., King, A. R., & Beuermann, K. 2000, A&A, 354, L37

Rey, S.-C., et al. 2005, ApJ, 619, L119

Roming, P. W. A., et al. 2005, Space Sci. Rev., 120, 95

Saha, A., Armandroff, T., Sawyer, D. G., & Corson, C. 2000, Proc. SPIE, 4008, 447

Saio, H., & Nomoto, K. 2004, ApJ, 615, 444

Schmidtke, P. C., & Cowley, A. P. 1996, AJ, 112, 167

Shirey, R. 2001, IAU Circ., 7659, 1

Šimon, V. 2003, A&A, 406, 613

Smirnova, O., & Alksnis, A. 2006, IBVS, 5720

Sparke, L. S., & Gallagher, J. S. 2007, Galaxies in the Universe: An Introduction (Cambridge: Cambridge Univ. Press)

Stiele, H., Pietsch, W., Haberl, F., & Freyberg, M. 2008, A&A, 480, 599

Sullivan, M., et al. 2006, ApJ, 648, 868

Supper, R., Hasinger, G., Pietsch, W., Truemper, J., Jain, A., Magnier, E. A., Lewin, W. H. G., & van Paradijs, J. 1997, A&A, 317, 328

Takei, D., Tsujimoto, M., Kitamoto, S., Morii, M., Ebisawa, K., Maeda, Y., & Miller, E. D. 2008, PASJ, 60, 231

Tavani, M., & Arons, J. 1997, ApJ, 477, 439

Thilker, D. A., et al. 2005, ApJ, 619, L67

Townsend, R. H. D., Owocki, S. P., & Howarth, I. D. 2004, MNRAS, 350, 189

Trudolyubov, S., Kotov, O., Priedhorsky, W., Cordova, F., & Mason, K. 2005, ApJ, 634, 314

Trudolyubov, S. P., & Priedhorsky, W. C. 2008, ApJ, 676, 1218

Unwin, S. C. 1980, MNRAS, 192, 243

van den Bergh, S. 1964, ApJS, 9, 65

van den Heuvel, E. P. J., Bhattacharya, D., Nomoto, K., & Rappaport, S. A. 1992, A&A, 262, 97

Vennes, S. 2000, A&A, 354, 995

Walborn, N. R. 1972, AJ, 77, 312

Waters, L. B. F. M., Pols, O. R., Hogeveen, S. J., Cote, J., & van den Heuvel, E. P. J. 1989, A&A, 220, L1

White, N. E., Giommi, P., Heise, J., Angelini, L., & Fantasia, S. 1995, ApJ, 445, L125

Williams, B. F., Garcia, M. R., McClintock, J. E., Primini, F. A., & Murray, S. S. 2006a, ApJ, 637, 479

Williams, B. F., Naik, S., Garcia, M. R., & Callanan, P. J. 2006b, ApJ, 643, 844

Yungelson, L. R. 2005, in Astrophysics and Space Science Library, Vol. 332, White Dwarfs: Cosmological and Galactic Probes, ed. E. M. Sion, S. Vennes, & H. L. Shipman (Dordrecht: Springer), 163